

TARM: A Turbo-type Algorithm for Affine Rank Minimization

Zhipeng Xue, Xiaojun Yuan, *Senior Member, IEEE*, Junjie Ma, and Yi Ma, *Fellow, IEEE*

Abstract—The affine rank minimization (ARM) problem arises in many real-world applications. The goal is to recover a low-rank matrix from a small amount of noisy affine measurements. The original problem is NP-hard, and so directly solving the problem is computationally prohibitive. Approximate low-complexity solutions for ARM have recently attracted much research interest. In this paper, we design an iterative algorithm for ARM based on message passing principles. The proposed algorithm is termed turbo-type ARM (TARM), as inspired by the recently developed turbo compressed sensing algorithm for sparse signal recovery. We show that, when the linear operator for measurement is right-orthogonally invariant (ROIL), a scalar function called state evolution can be established to accurately predict the behaviour of the TARM algorithm. We also show that TARM converges much faster than the counterpart algorithms for low-rank matrix recovery. We further extend the TARM algorithm for matrix completion, where the measurement operator corresponds to a random selection matrix. We show that, although the state evolution is not accurate for matrix completion, the TARM algorithm with carefully tuned parameters still significantly outperforms its counterparts.

Index Terms—Low-rank matrix recovery, matrix completion, affine rank minimization, state evolution, low-rank matrix denoising.

I. INTRODUCTION

Low-rank matrices have extensive applications in real-world applications including remote sensing, recommendation systems, global positioning, and system identification. In these applications, a fundamental problem is to recover an unknown matrix from a small number of observations by exploiting its low-rank property [1], [2]. In specific, we consider a rank- r matrix $\mathbf{X}^* \in \mathbb{R}^{n_1 \times n_2}$ with the integers r , n_1 , and n_2 satisfying $r \ll n_1$ and $r \ll n_2$. We aim to recover \mathbf{X}^* from an affine measurement given by

$$\mathbf{y} = \mathcal{A}(\mathbf{X}^*) \in \mathbb{R}^m \quad (1)$$

where $\mathcal{A} : \mathbb{R}^{n_1 \times n_2} \rightarrow \mathbb{R}^m$ is a linear map with $m < n_1 n_2 = n$. When \mathcal{A} is a general linear operator such as Gaussian operators and partial orthogonal operators, we refer to the problem as *low-rank matrix recovery*; when \mathcal{A} is a selector that outputs a subset of the entries of \mathbf{X}^* , we refer to the problem as *matrix completion*.

The problem can be formally cast as affine rank minimization (ARM):

$$\begin{aligned} \min_{\mathbf{X}} \quad & \text{rank}(\mathbf{X}) \\ \text{s.t.} \quad & \mathbf{y} = \mathcal{A}(\mathbf{X}). \end{aligned} \quad (2)$$

Problem (2) is NP-hard, and so solving (2) is computationally prohibitive. To reduce complexity, a popular alternative to (2) is the following nuclear norm minimization (NNM) problem:

$$\begin{aligned} \min_{\mathbf{X}} \quad & \|\mathbf{X}\|_* \\ \text{s.t.} \quad & \mathbf{y} = \mathcal{A}(\mathbf{X}). \end{aligned} \quad (3)$$

In [3], Recht et al. proved that when the restricted isometry property (RIP) holds for the linear operator \mathcal{A} , the ARM problem in (2) is equivalent to the NNM problem in (3). The NNM problem can be solved by semidefinite programming (SDP). Existing convex solvers, such as the interior point method [4], can be employed to find a solution in polynomial time. However, SDP is still computationally involving, especially when applied to large-scale problems with high dimensional data. To address this issue, low-cost iterative methods, such as the singular value thresholding (SVT) method [5] and the proximal gradient algorithm [6], have been proposed to further reduce complexity at the cost of a certain amount of performance degradation.

In real-world applications, perfect measurements are rare, and noise is naturally introduced in the measurement process. That is, we want to recover \mathbf{X}^* from a noisy measurement of

$$\mathbf{y} = \mathcal{A}(\mathbf{X}^*) + \mathbf{n} \quad (4)$$

where $\mathbf{n} \in \mathbb{R}^m$ is a Gaussian noise with zero-mean and covariance $\sigma^2 \mathbf{I}$ and is independent of $\mathcal{A}(\mathbf{X}^*)$. To recover the low-rank matrix \mathbf{X}^* from (4), we turn to the following stable formulation of the ARM problem:

$$\begin{aligned} \min_{\mathbf{X}} \quad & \|\mathbf{y} - \mathcal{A}(\mathbf{X})\|_2^2 \\ \text{s.t.} \quad & \text{rank}(\mathbf{X}) \leq r. \end{aligned} \quad (5)$$

The problem in (5) is still NP-hard and difficult to solve. Several suboptimal algorithms have been proposed to yield approximate solutions to (5). For example, the author in [10] proposed an alternation minimization method to factorize rank- r matrix \mathbf{X}^* as the product of two matrices with dimension $n_1 \times r$ and $r \times n_2$ respectively. This method is more efficient in storage than SDP and SVT methods, especially when large-dimension low-rank matrices are involved. A second approach borrows the idea of iterative hard thresholding (IHT) for compressed sensing. For example, the singular value projection (SVP) algorithm [7] for stable ARM can be viewed as a counterpart of the IHT algorithm [9] for compressed sensing. SVP solves the stable ARM problem by combining the projected gradient method with singular value decomposition (SVD). Improved version of SVP, termed normalized IHT (NIHT) [8], adaptively selects the step size

of the gradient descent step of SVP, rather than uses a fixed step size. These algorithms involve a projection step which projects a matrix into a low-rank space using truncated SVD. In [21], a Riemannian method, termed RGrad, was proposed to extend NIHT by projecting the search direction of gradient descent into a low dimensional space. Compared with the alternation minimization method, these IHT-based algorithms exhibit better convergence performance with lower computational complexity. Furthermore, the convergence of these IHT-based algorithms are guaranteed when a certain restricted isometry property (RIP) holds [7], [8], [21].

In this paper, we aim to design low-complexity iterative algorithms to solve the stable ARM problem based on message-passing principles [11], a perspective different from the existing approaches mentioned above. In specific, we propose a novel turbo-type algorithm, termed turbo-type affine rank minimization (TARM), for solving the stable ARM problem, as inspired by the turbo compressed-sensing (Turbo-CS) algorithm for sparse signal recovery [11], [12]. Interestingly, although TARM is designed based on the idea of message passing, the resultant algorithm bears a similar structure to the gradient-based algorithms such as SVP and NIHT. A key difference of TARM from SVP and NIHT resides in an extra step in TARM for the calculation of the so-called extrinsic messages. With this extra step, TARM is able to find a better descendent direction for each iteration, so as to achieve a much higher convergence rate than SVP and NIHT. For low-rank matrix recovery, we establish a state evolution technique to characterize the behaviour of the TARM algorithm when the linear operator \mathcal{A} is right-orthogonally invariant (ROIL). We show that the state evolution accurately predicts the performance of the TARM algorithm. We also show that TARM converges much faster than other existing algorithms including SVP, NIHT, and RGrad. We further extend the TARM algorithm for matrix completion. We show that, although the state evolution cannot accurately predict the performance any more, the TARM algorithm with carefully tuned parameters still considerably outperforms its counterparts with comparable computational complexity.

II. THE TARM ALGORITHM

A. Algorithm Description

In this section, we describe our proposed algorithm for affine rank minimization. The algorithm is inspired by the idea of turbo compressed sensing [12], [11], hence the name turbo-type affine rank minimization (TARM).

The diagram of TARM is illustrated in Fig. 1. There are two concatenated modules in TARM, namely, Module A and Module B. Module A estimates the low-rank matrix \mathbf{X}^* via a linear estimator $\mathcal{E}(\cdot)$ based on the observation \mathbf{y} and the input \mathbf{X} . Then the function $\mathcal{E}^{ext}(\cdot)$, which linearly combines $\mathcal{E}(\mathbf{X})$ and \mathbf{X} , is employed to decorrelate the input and output estimation errors of Module A. The superscript “ext” stands for extrinsic, since the output of $\mathcal{E}^{ext}(\cdot)$ is referred to as an extrinsic message. Module B has a similar structure as Module A does. In Module B, the output \mathbf{R} of Module A is passed to a denoiser $\mathcal{D}(\cdot)$ which suppresses the estimation error by

exploiting the low-rank structure of \mathbf{X}^* . The denoised output \mathbf{Z} is then passed to a function $\mathcal{D}^{ext}(\cdot)$ which linearly combines \mathbf{Z} and \mathbf{R} for the decorrelation of input output errors. The two modules are executed iteratively to refine the estimates. Note that the TARM diagram in Fig. 1 is a matrix analogy of the Turbo-CS algorithm in Fig. 2 of [12].

The details of TARM are presented in Algorithm 1. We use index t to denote the t -th iteration. There are three main steps at each iteration of TARM. The first step (Line 3 of Algorithm 1) is a linear estimation step which corresponds to Module A in Fig. 1. This step combines $\mathcal{E}(\cdot)$ and $\mathcal{E}^{ext}(\cdot)$ since both are linear functions. Interestingly, this step can be interpreted as a gradient descent step for problem (5), where the parameter μ_t is the step size at the t -th iteration. In this sense, the TARM algorithm described here is closely related to the gradient-descent based SVP algorithm in [7] and the NIHT algorithm in [8]. The second step (Line 4 of Algorithm 1) processes $\mathbf{R}^{(t)}$ with a denoiser $\mathcal{D}(\cdot)$. This step corresponds to the denoiser in Module B of TARM. There are various choices of $\mathcal{D}(\cdot)$ in the literature, such as the best rank- r approximation [13] and the singular value thresholding (SVT) denoiser [14]. In this paper, we focus on the best rank- r approximation defined by

$$\mathcal{D}(\mathbf{R}) = \sum_{i=1}^r \sigma_i \mathbf{u}_i \mathbf{v}_i^T \quad (6)$$

where σ_i , \mathbf{u}_i , and \mathbf{v}_i are respectively the i -th singular value and the corresponding left and right singular vectors of the input \mathbf{R} . We will show that, with this choice of $\mathcal{D}(\cdot)$, Module B allows an analytical characterization of its input output behavior. The third step (Line 5 of Algorithm 1) corresponds to function $\mathcal{D}^{ext}(\cdot)$ which is a linear combination of $\mathbf{R}^{(t)}$ and $\mathbf{Z}^{(t)}$ with the coefficients specified by c_t and α_t .

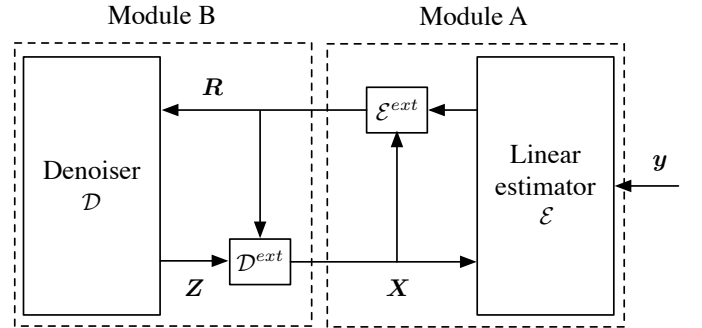


Fig. 1. The diagram of the TARM algorithm.

Algorithm 1 TARM for affine rank minimization

Input: $\mathcal{A}, \mathbf{y}, \mathbf{X}^{(0)} = \mathbf{0}, t = 0$
1: **while** the stopping criterion is not met **do**
2: $t = t + 1$
3: $\mathbf{R}^{(t)} = \mathbf{X}^{(t-1)} + \mu_t \mathcal{A}^T(\mathbf{y} - \mathcal{A}(\mathbf{X}^{(t-1)}))$
4: $\mathbf{Z}^{(t)} = \mathcal{D}(\mathbf{R}^{(t)})$
5: $\mathbf{X}^{(t)} = c_t(\mathbf{Z}^{(t)} - \alpha_t \mathbf{R}^{(t)})$
6: **end while**
Output: $\mathbf{Z}^{(t)}$

B. Determining the Parameters of TARM

In this section, we discuss how to determine the parameters $\{\mu_t\}$, $\{c_t\}$, and $\{\alpha_t\}$. We first note that when $c_t = 1$ and $\alpha_t = 0$ for any t , the algorithm reduces to the SVP or NIHT algorithm (depending on the choice of μ_t). As such, the key difference of TARM from SVP and NIHT resides in the choice of these parameters. By optimizing these parameters, the TARM algorithm aims to find a much steeper descendent direction for each iteration, so as to achieve a convergence rate much higher than SVP and NIHT. In specific, we follow the turbo principle [12], [11], a special form of the more general message passing principle, to determine these parameters. That is, for each iteration t , $\{\mu_t, c_t, \alpha_t\}$ need to satisfy the following three conditions:

- Condition 1:

$$\langle \mathbf{R}^{(t)} - \mathbf{X}^*, \mathbf{X}^{(t-1)} - \mathbf{X}^* \rangle = 0, \quad (7)$$

- Condition 2:

$$\langle \mathbf{R}^{(t)} - \mathbf{X}^*, \mathbf{X}^{(t)} - \mathbf{X}^* \rangle = 0, \quad (8)$$

- Condition 3: For given $\mathbf{X}^{(t-1)}$,

$$\|\mathbf{X}^{(t)} - \mathbf{X}^*\|_F^2 \text{ is minimized under (7) and (8).} \quad (9)$$

In the above, Condition 1 ensures that the input and output estimation errors of Module A are uncorrelated. Similarly, Condition 2 ensures that the input and output estimation errors of Module B are uncorrelated. Condition 3 ensures that the output estimation error of Module B is minimized over $\{\mu_t, c_t, \alpha_t\}$ for each iteration t . Note that in graphical-model based message passing, the out-going message on an edge is required to be independent of the incoming message on the edge. Since uncorrelatedness implies independence for Gaussian random variables, (7) and (8) can be seen as necessary conditions for Gaussian message passing. In this sense, the minimization in (9) can be interpreted as finding the best estimate of \mathbf{X}^* for each iteration under the Gaussian message passing framework.

We have the following lemma, with the proof given in Appendix A.

Lemma 1. *If Conditions 1-3 hold, then*

$$\mu_t = \frac{\|\mathbf{X}^{(t-1)} - \mathbf{X}^*\|_F^2}{\langle \mathcal{A}(\mathbf{X}^{(t-1)} - \mathbf{X}^*) - \mathbf{n}, \mathcal{A}(\mathbf{X}^{(t-1)} - \mathbf{X}^*) \rangle} \quad (10a)$$

$$\alpha_t = \frac{-b_t \pm \sqrt{b_t^2 - 4a_t d_t}}{2a_t} \quad (10b)$$

$$c_t = \frac{\langle \mathbf{Z}^{(t)} - \alpha_t \mathbf{R}^{(t)}, \mathbf{R}^{(t)} \rangle}{\|\mathbf{Z}^{(t)} - \alpha_t \mathbf{R}^{(t)}\|_F^2}, \quad (10c)$$

with

$$a_t = \|\mathbf{R}^{(t)}\|_F^2 \|\mathbf{R}^{(t)} - \mathbf{X}^*\|_F^2 \quad (11a)$$

$$b_t = -\|\mathbf{R}^{(t)}\|_F^2 \langle \mathbf{R}^{(t)} - \mathbf{X}^*, \mathbf{Z}^{(t)} \rangle - \|\mathbf{Z}^{(t)}\|_F^2 \|\mathbf{R}^{(t)} - \mathbf{X}^*\|_F^2 + \|\mathbf{Z}^{(t)}\|_F^2 \langle \mathbf{R}^{(t)} - \mathbf{X}^*, \mathbf{X}^* \rangle \quad (11b)$$

$$d_t = \|\mathbf{Z}^{(t)}\|_F^2 \langle \mathbf{R}^{(t)} - \mathbf{X}^*, \mathbf{Z}^{(t)} - \mathbf{X}^* \rangle. \quad (11c)$$

Remark 1. In (10b), α_t has two possible choices and only one of them minimizes the error in (9). From the discussion below (32), minimizing the square error in (9) is equivalent to minimizing $\|\mathbf{X}^{(t)} - \mathbf{R}^{(t)}\|_F^2$. We have

$$\begin{aligned} & \|\mathbf{X}^{(t)} - \mathbf{R}^{(t)}\|_F^2 \\ &= \|c_t(\mathbf{Z}^{(t)} - \alpha_t \mathbf{R}^{(t)}) - \mathbf{R}^{(t)}\|_F^2 \end{aligned} \quad (12a)$$

$$= \left\| \frac{\langle \mathbf{Z}^{(t)} - \alpha_t \mathbf{R}^{(t)}, \mathbf{R}^{(t)} \rangle}{\|\mathbf{Z}^{(t)} - \alpha_t \mathbf{R}^{(t)}\|_F^2} (\mathbf{Z}^{(t)} - \alpha_t \mathbf{R}^{(t)}) - \mathbf{R}^{(t)} \right\|_F^2 \quad (12b)$$

$$= -\frac{\langle \mathbf{Z}^{(t)} - \alpha_t \mathbf{R}^{(t)}, \mathbf{R}^{(t)} \rangle^2}{\|\mathbf{Z}^{(t)} - \alpha_t \mathbf{R}^{(t)}\|_F^2} + \|\mathbf{R}^{(t)}\|_F^2 \quad (12c)$$

where (12a) follows from substituting $\mathbf{X}^{(t)}$ in Line 5 of Algorithm 1, and (12b) follows by substituting c_t in (10c). Since $\|\mathbf{R}^{(t)}\|_F^2$ is invariant to α_t , minimizing $\|\mathbf{X}^{(t)} - \mathbf{R}^{(t)}\|_F^2$ is equivalent to maximizing $\frac{\langle \mathbf{Z}^{(t)} - \alpha_t \mathbf{R}^{(t)}, \mathbf{R}^{(t)} \rangle^2}{\|\mathbf{Z}^{(t)} - \alpha_t \mathbf{R}^{(t)}\|_F^2}$. We choose α_t that gives a larger value of $\frac{\langle \mathbf{Z}^{(t)} - \alpha_t \mathbf{R}^{(t)}, \mathbf{R}^{(t)} \rangle^2}{\|\mathbf{Z}^{(t)} - \alpha_t \mathbf{R}^{(t)}\|_F^2}$.

Remark 2. Similarly to SVP [7] and NIHT [8], the convergence of TARM can be analyzed by assuming that the linear operator \mathcal{A} satisfies the restricted isometry property (RIP). The convergence rate of TARM is much faster than those of NIHT and SVP (provided that $\{\alpha_t\}$ are sufficiently small). More detailed discussions are presented in Appendix B.

We emphasize that the parameters μ_t, α_t , and c_t in (10) are actually difficult to evaluate since \mathbf{X}^* and \mathbf{n} are unknown. This means that Algorithm 1 cannot rely on (10) to determine μ_t, α_t and c_t . In the following, we focus on how to approximately evaluate these parameters to yield practical algorithms. Based on different choices of the linear operator \mathcal{A} , our discussions are divided into two parts, namely, low-rank matrix recovery and matrix completion.

III. LOW-RANK MATRIX RECOVERY

A. Preliminaries

In this section, we consider recovering \mathbf{X}^* from measurement in (5) when the linear operator \mathcal{A} is right-orthogonally invariant. Denote the vector form of \mathbf{X} by $\mathbf{x} = \text{vec}(\mathbf{X}) = [\mathbf{x}_1^T, \mathbf{x}_2^T, \dots, \mathbf{x}_n^T]^T$, where \mathbf{x}_i is the i th column of \mathbf{X} . The linear operator \mathcal{A} can be generally expressed as $\mathcal{A}(\mathbf{X}) = \text{Avec}(\mathbf{X}) = \mathbf{A}\mathbf{x}$ where $\mathbf{A} \in \mathbb{R}^{m \times n}$ is a matrix representation of \mathcal{A} . The adjoint operator $\mathcal{A}^T : \mathbb{R}^m \rightarrow \mathbb{R}^{n_1 \times n_2}$ is defined by the transpose of \mathbf{A} with $\mathbf{x}' = \text{vec}(\mathbf{X}') = \text{vec}(\mathcal{A}^T(\mathbf{y}')) = \mathbf{A}^T \mathbf{y}'$.

Definition 1. Consider a linear operator \mathcal{A} with matrix form \mathbf{A} , the SVD of \mathbf{A} is $\mathbf{A} = \mathbf{U}_A \Sigma_A \mathbf{V}_A^T$, where \mathbf{U}_A and \mathbf{V}_A are orthogonal matrices and Σ_A is a diagonal matrix. If \mathbf{V}_A is a Haar distributed random matrix independent of Σ_A , we say that \mathcal{A} is a right-orthogonally invariant linear (ROIL) operator.

We focus on two types of ROIL operators: partial orthogonal ROIL operators where the matrix form of \mathcal{A} satisfies $\mathbf{A}\mathbf{A}^T = \mathbf{I}$, and Gaussian ROIL operators where the elements of \mathbf{A} are

i.i.d. Gaussian with zero mean. For convenience of discussion, the linear operator \mathcal{A} is normalized such that the length of each row of \mathbf{A} is 1. It is worth noting that from the perspective of the algorithm, \mathbf{A} is deterministic since \mathbf{A} is known by the algorithm. However, the randomness of \mathbf{A} has impact on parameter design and performance analysis, as detailed in what follows.

B. Parameter Design

We now determine the parameters in (10) when ROIL operators are involved. We show that (10) can be approximately evaluated without the knowledge of \mathbf{X}^* . Since $\{c_t\}$ in (10c) can be readily computed given $\{\alpha_t\}$, we focus on the calculation of $\{\mu_t\}$ and $\{\alpha_t\}$.

We start with μ_t . From (10a), we have

$$\mu_t = \frac{\|\mathbf{X}^{(t-1)} - \mathbf{X}^*\|_F^2}{\langle \mathcal{A}(\mathbf{X}^{(t-1)} - \mathbf{X}^*) - \mathbf{n}, \mathcal{A}(\mathbf{X}^{(t-1)} - \mathbf{X}^*) \rangle} \quad (13a)$$

$$\approx \frac{\|\mathbf{X}^{(t-1)} - \mathbf{X}^*\|_F^2}{\|\mathcal{A}(\mathbf{X}^{(t-1)} - \mathbf{X}^*)\|_2^2} \quad (13b)$$

$$= \frac{1}{\|\mathcal{A}(\frac{\mathbf{X}^{(t-1)} - \mathbf{X}^*}{\|\mathbf{X}^{(t-1)} - \mathbf{X}^*\|_F})\|_2^2} \quad (13c)$$

$$= \frac{1}{\tilde{\mathbf{x}}^T \mathbf{V}_A \Sigma_A^T \Sigma_A \mathbf{V}_A^T \tilde{\mathbf{x}}} \quad (13d)$$

$$= \frac{1}{\mathbf{v}_A^T \Sigma_A^T \Sigma_A \mathbf{v}_A} \quad (13e)$$

$$\approx \frac{n}{m} \quad (13f)$$

where (13b) follows from $\langle \mathbf{n}, \mathcal{A}(\mathbf{X}^{(t-1)} - \mathbf{X}^*) \rangle \approx 0$, (13d) follows by utilizing the matrix form of \mathcal{A} and $\tilde{\mathbf{x}} = \frac{\text{vec}(\mathbf{X}^{(t-1)} - \mathbf{X}^*)}{\|\mathbf{X}^{(t-1)} - \mathbf{X}^*\|_F}$, and (13e) follows by letting $\mathbf{v}_A = \mathbf{V}_A^T \tilde{\mathbf{x}}$. As \mathcal{A} is a ROIL operator, \mathbf{V}_A is haar distributed and is approximately independent of $\tilde{\mathbf{x}}$, implying that \mathbf{v}_A is a unit vector uniformly distributed over the sphere $\|\mathbf{v}_A\|_2 = 1$. Then, the last step of (13) follows by noting $\text{Tr}(\Sigma_A^T \Sigma_A) = m$.

We next consider the approximation of α_t . We first note

$$\langle \mathbf{R}^{(t)} - \mathbf{X}^*, \mathbf{X}^{(t)} - \mathbf{X}^* \rangle \quad (14a)$$

$$= \langle \mathbf{R}^{(t)} - \mathbf{X}^*, c_t(\mathbf{Z}^{(t)} - \alpha_t \mathbf{R}^{(t)}) - \mathbf{X}^* \rangle \quad (14b)$$

$$\approx c_t \langle \mathbf{R}^{(t)} - \mathbf{X}^*, \mathbf{Z}^{(t)} - \alpha_t \mathbf{R}^{(t)} \rangle \quad (14c)$$

where (14a) follows by substituting $\mathbf{X}^{(t)}$ in line 5 of Algorithm 1, and (14b) follows from $\langle \mathbf{R}^{(t)} - \mathbf{X}^*, \mathbf{X}^* \rangle \approx 0$ implying that the error $\mathbf{R}^{(t)} - \mathbf{X}^*$ is uncorrelated with the original signal \mathbf{X}^* . Combining (14) and Condition 2 in (8), we have

$$\alpha_t = \frac{\langle \mathbf{R}^{(t)} - \mathbf{X}^*, \mathbf{Z}^{(t)} \rangle}{\langle \mathbf{R}^{(t)} - \mathbf{X}^*, \mathbf{R}^{(t)} \rangle} \quad (15a)$$

$$\approx \frac{\langle \mathbf{R}^{(t)} - \mathbf{X}^*, \mathcal{D}(\mathbf{R}^{(t)}) \rangle}{\langle \mathbf{R}^{(t)} - \mathbf{X}^*, \mathbf{R}^{(t)} - \mathbf{X}^* \rangle} \quad (15b)$$

$$\approx \frac{\langle \mathbf{R}^{(t)} - \mathbf{X}^*, \mathcal{D}(\mathbf{R}^{(t)}) \rangle}{nv_t} \quad (15c)$$

$$\approx \frac{1}{n} \sum_{i,j} \frac{\partial \mathcal{D}(\mathbf{R}^{(t)})}{\partial R_{i,j}^{(t)}} \quad (15d)$$

$$= \frac{1}{n} \text{div}(\mathcal{D}(\mathbf{R}^{(t)})) \quad (15e)$$

where (15b) follows from $\mathbf{Z}^{(t)} = \mathcal{D}(\mathbf{R}^{(t)})$ and $\langle \mathbf{R}^{(t)} - \mathbf{X}^*, \mathbf{X}^* \rangle \approx 0$, (15c) follows from the Gaussian approximation that the elements of $\mathbf{R}^{(t)} - \mathbf{X}^*$ are i.i.d. Gaussian with zero mean and variance v_t , (15d) follows from Stein's lemma [20] since we approximate the entries of $\mathbf{R}^{(t)} - \mathbf{X}^*$ as i.i.d. Gaussian distributed, and (15e) is from the definition of the divergence $\text{div}(\cdot)$.

C. State Evolution

We now characterize the performance of TARM for low-rank matrix recovery. Recall that some assumptions are involved in determining the algorithm parameters in the preceding subsection. We formally present these assumptions as follows.

Assumption 1. For each iteration t , the orthogonal matrix \mathbf{V}_A is independent of Module A's input estimation error $\mathbf{X}^{(t-1)} - \mathbf{X}^*$.

Assumption 2. For each iteration t , the output error of Module A, given by $\mathbf{R}^{(t)} - \mathbf{X}^*$, resembles an i.i.d. Gaussian noise, i.e., the elements of $\mathbf{R}^{(t)} - \mathbf{X}^*$ are independently and identically drawn from $\mathcal{N}(0, v_t)$, where v_t is the output variance of Module A at iteration t .

The above two assumptions will be verified by the numerical results presented in the next subsection. Similar assumptions have been introduced in the design of Turbo-CS in [11] (see also [15]). Later, these assumptions were rigorously analyzed in [16], [17] using the conditioning technique [18]. Based on that, state evolution was established to characterize the behavior of the Turbo-CS algorithm. However, the analyses in [16], [17] are focused on the case that the denoiser $\mathcal{D}(\cdot)$ is separable, i.e., the function $\mathcal{D}(\cdot)$ is individually applied to each element of the input, while the denoisers involved here (such as the best-rank- r approximation in (6)) are non-separable. Therefore, the technique in [16]-[18] cannot be directly applied here. The recent work [19] on state evolution of AMP for non-separable denoisers may shed some light on a possible rigorous justification of the assumptions. In this paper, we establish state evolution based on the two assumptions. We leave the rigorous proof (without imposing the assumptions) as future work.

Assumptions 1 and 2 allow to decouple Module A and Module B in the analysis of the TARM algorithm. We derive

two mean square error (MSE) transfer functions, one for each module, to characterize the behavior of the TARM algorithm.

We first consider the MSE behavior of Module A. Denote the output MSE of Module A at iteration t by

$$MSE_A^{(t)} = \frac{1}{n} \|\mathbf{R}^{(t)} - \mathbf{X}^*\|_F^2. \quad (16)$$

The following theorem gives the asymptotic MSE of Module A when the dimension of \mathbf{X}^* goes to infinity, with the proof given in Appendix C.

Theorem 1. Assume that Assumption 1 holds, and let $\mu = \frac{n}{m}$. Then,

$$MSE_A^{(t)} \xrightarrow{a.s.} f(\tau_t) \quad (17)$$

as $m, n \rightarrow \infty$ with $\frac{m}{n} \rightarrow \delta$, where $\frac{1}{n} \|\mathbf{X}^{(t-1)} - \mathbf{X}^*\|_F^2 \rightarrow \tau_t$ as $n \rightarrow \infty$. For partial orthogonal ROIL operator \mathcal{A} ,

$$f(\tau) = \left(\frac{1}{\delta} - 1 \right) \tau + \sigma^2 \quad (18a)$$

and for Gaussian ROIL operator \mathcal{A} ,

$$f(\tau) = \frac{1}{\delta} \tau + \sigma^2. \quad (18b)$$

We now consider the MSE behavior of Module B. We start with the following useful lemma, with the proof given in Appendix D.

Lemma 2. Assume that $\mathbf{R}^{(t)}$ satisfies Assumption 2, $\|\mathbf{X}^*\|_F^2 = n$, and the empirical distribution of eigenvalue θ of $\frac{1}{n_2} \mathbf{X}^{*T} \mathbf{X}^*$ converges almost surely to the density function $p(\theta)$ as $n_1, n_2, r \rightarrow \infty$ with $\frac{n_1}{n_2} \rightarrow \rho$, $\frac{r}{n_2} \rightarrow \lambda$. Then,

$$\alpha_t \xrightarrow{a.s.} \alpha(v_t) \quad (19a)$$

$$c_t \xrightarrow{a.s.} c(v_t) \quad (19b)$$

as $n_1, n_2, r \rightarrow \infty$ with $\frac{n_1}{n_2} \rightarrow \rho$, $\frac{r}{n_2} \rightarrow \lambda$, where

$$\alpha(v) = \left| 1 - \frac{1}{\rho} \right| \lambda + \frac{1}{\rho} \lambda^2 + 2 \left(\min \left(1, \frac{1}{\rho} \right) - \frac{\lambda}{\rho} \right) \lambda \Delta_1(v) \quad (20a)$$

$$c(v) = \frac{1 + \lambda(1 + \frac{1}{\rho})v + \lambda v^2 \Delta_2 - \alpha(v)(1 + v)}{(1 - 2\alpha(v))(1 + \lambda(1 + \frac{1}{\rho})v + \lambda v^2 \Delta_2) + \alpha(v)^2(1 + v)} \quad (20b)$$

with Δ_1 and Δ_2 defined by

$$\Delta_1(v) = \int_0^\infty \frac{(v + \theta^2)(\rho v + \theta^2)}{(\sqrt{\rho v} - \theta^2)^2} p(\theta) d\theta \quad (21a)$$

$$\Delta_2 = \int_0^\infty \frac{1}{\theta^2} p(\theta) d\theta. \quad (21b)$$

Denote the output MSE of Module B at iteration t by

$$MSE_B^{(t)} = \frac{1}{n} \|\mathbf{X}^{(t)} - \mathbf{X}^*\|_F^2. \quad (22)$$

The output MSE of Module B is characterized by the following theorem.

Theorem 2. Assume that Assumption 2 holds, and let $\|\mathbf{X}^*\|_F^2 = n$. Then, the output MSE of Module B

$$MSE_B^{(t)} \xrightarrow{a.s.} g(v_t) \triangleq \frac{v_t - \lambda \left(1 + \frac{1}{\rho} \right) v_t - \lambda v_t^2 \Delta_2}{\frac{v_t - \lambda \left(1 + \frac{1}{\rho} \right) v_t - \lambda v_t^2 \Delta_2}{1 + \lambda \left(1 + \frac{1}{\rho} \right) v_t + \lambda v_t^2 \Delta_2} \alpha(v_t)^2 + (1 - \alpha(v_t))^2} - v_t \quad (23)$$

as $n_1, n_2, r \rightarrow \infty$ with $\frac{n_1}{n_2} \rightarrow \rho$, $\frac{r}{n_2} \rightarrow \lambda$, where α and Δ_2 are given in Lemma 2, and $\frac{1}{n} \|\mathbf{R}^{(t)} - \mathbf{X}^*\|_F^2 \xrightarrow{a.s.} v_t$.

Remark 3. Δ_1 and Δ_2 in (21) may be difficult to obtain since $p(\theta)$ is usually unknown in practical scenarios. We now introduce an approximate MSE expression that does not depend on $p(\theta)$:

$$g(v_t) \approx \bar{g}(v_t) \triangleq \frac{v_t - \lambda \left(1 + \frac{1}{\rho} \right) v_t}{(1 - \alpha)^2} - v_t \quad (24)$$

where $\alpha = \alpha(0) = \left| 1 - \frac{1}{\rho} \right| \lambda - \frac{1}{\rho} \lambda^2 + 2 \min \left(1, \frac{1}{\rho} \right) \lambda$. Compared with $g(v_t)$, $\bar{g}(v_t)$ omits two terms $-\lambda v_t^2 \Delta_2$ and $\frac{v_t - \lambda \left(1 + \frac{1}{\rho} \right) v_t - \lambda v_t^2 \Delta_2}{1 + \lambda \left(1 + \frac{1}{\rho} \right) v_t + \lambda v_t^2 \Delta_2} \alpha(v_t)^2$ and replaces $\alpha(v_t)$ by α . Recall that v_t is the mean square error at the t -iteration. As the iteration proceeds, we have $v_t \ll 1$, and hence $g(v_t)$ can be well approximated by $\bar{g}(v_t)$, as seen later from Fig. 3.

Combining Theorems 1 and 2, we can characterize the MSE evolution of TARM by

$$v_t = f(\tau_t) \quad (25a)$$

$$\tau_{t+1} = g(v_t). \quad (25b)$$

The fixed point of TARM's MSE evolution in (25) is given by

$$\tau^* = g(f(\tau^*)). \quad (26)$$

The above fixed point equation can be used to analysis the phase transition curves of the TARM algorithm. It is clear that the fixed point τ^* of (26) is a function of $\{\delta, \rho, \lambda, \Delta, \sigma\}$. For any given $\{\delta, \rho, \lambda, \Delta, \sigma\}$, we say that the TARM algorithm is successful if the corresponding τ^* is below a certain predetermined threshold. The critical values of $\{\delta, \rho, \lambda, \Delta, \sigma\}$ define the phase transition curves of the TARM algorithm.

D. Numerical Results

Some simulation settings are as follows. For the case of partial orthogonal ROIL operators, we generate a partial orthogonal ROIL operator with the matrix form $\mathbf{A} = \mathbf{S}\mathbf{W}$, where $\mathbf{S} \in \mathbb{R}^{m \times n}$ is a random perturbation matrix and $\mathbf{W} \in \mathbb{R}^{n \times n}$ is a discrete cosine transform (DCT) matrix. For the case of Gaussian ROIL operators, we generate an i.i.d. Gaussian random matrix of size $m \times n$ with elements drawn from $\mathcal{N}(0, \frac{1}{n})$. The rank- r matrix $\mathbf{X}^* \in \mathbb{R}^{n_1 \times n_2}$ is generated by the product of two i.i.d. Gaussian matrices of size $n_1 \times r$ and $r \times n_2$.

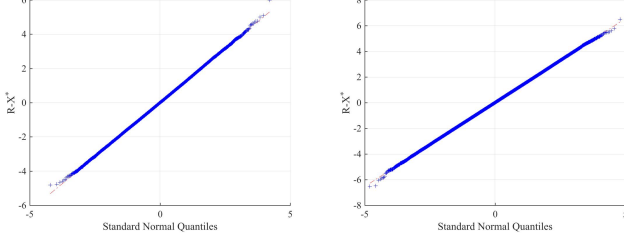


Fig. 2. The QQplots of the output error of Module B in the 2nd iteration of TARM. Left: \mathcal{A} is a Gaussian ROIL operator. Right: \mathcal{A} is a partial orthogonal ROIL operator. Simulation settings: $n_1 = 100, n_2 = 120, \frac{m}{n_1 n_2} = 0.3, \frac{r}{n_2} = 0.25, \sigma^2 = 0$.

1) *Verification of the assumptions:* We first verify Assumption 1 using Table I. Recall that if Assumption 1 holds, the approximations in the calculation of μ_t in (13) become accurate. Thus, we verify Assumption 1 by comparing the value of μ_t calculated by (10a) with $\frac{n}{m}$ by (13). We record the μ_t of the first 8 iterations of TARM in Table I for low-rank matrix recovery with a partial orthogonal ROIL operator. As shown in Table I, the approximation $\mu_t = \frac{n}{m}$ is close to the real value calculated by (10a) which verifies Assumption 1. We then verify Assumption 2 using Fig. 2, where we plot the QQplots of the input estimation errors of Module A with partial orthogonal and Gaussian ROIL operators. The QQplots show that the output errors of Module A closely follow a Gaussian distribution, which agrees with Assumption 2.

2) *State evolution:* We now verify the state evolution of TARM given in (25). We plot the simulation performance of TARM and the predicted performance by the state evolution in Fig. 3. From the two subfigures in Fig. 3, we see that the state evolution of TARM is accurate when the dimension of \mathbf{X}^* is large enough for both partial orthogonal and Gaussian ROIL operators. We also see that the state evolution with $g(\cdot)$ replaced by the approximation in (24) (referred to as "Approximation" in Fig. 3) provides reasonably accurate performance predictions. This makes the upper bound very useful since it does not require the knowledge of the singular value distribution of \mathbf{X}^* .

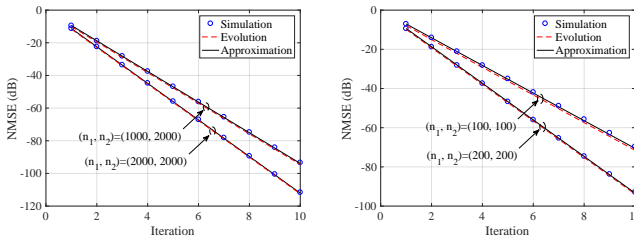


Fig. 3. Left: State evolution of TARM for partial orthogonal ROIL operator. $r = 40, m/n = m/(n_1 n_2) = 0.35, \sigma^2 = 0$. The size of \mathbf{X}^* is shown in the plot. Right: State evolution of TARM for Gaussian ROIL operator. $r = 4, m/n = 0.35, \sigma^2 = 0$. The size of \mathbf{X}^* is shown in the plot.

3) *Performance comparisons:* We compare TARM with the existing state-of-the-art algorithms for low-rank matrix recovery with partial orthogonal and Gaussian ROIL operators. The following algorithms are involved: singular value projection

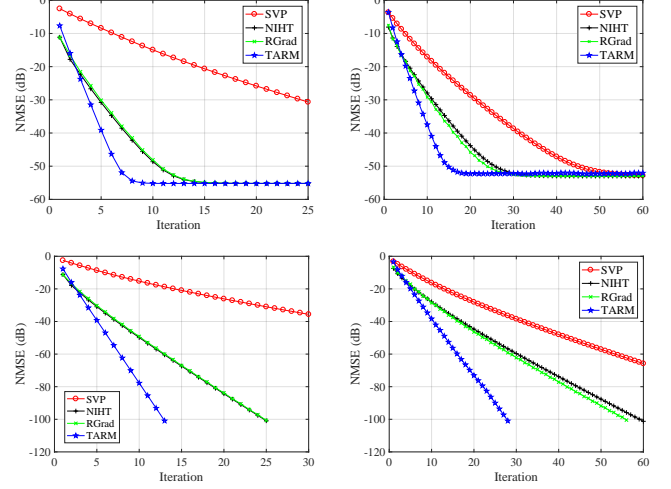


Fig. 4. Comparison of algorithms. Top left: \mathcal{A} is a partial orthogonal ROIL operator with $n_1 = n_2 = 1000, r = 50, m/n = 0.39, \sigma^2 = 10^{-5}$. Top right: \mathcal{A} is a random Gaussian ROIL operator with $n_1 = n_2 = 80, r = 10, p = (n_1 + n_2 - r) \times r, m/p = 3, \sigma^2 = 10^{-5}$. Bottom left: \mathcal{A} is a random Gaussian ROIL operator with $n_1 = n_2 = 80, r = 10, p = (n_1 + n_2 - r) \times r, m/p = 3, \sigma^2 = 0$. Bottom right: \mathcal{A} is a random Gaussian ROIL operator with $n_1 = n_2 = 80, r = 10, p = (n_1 + n_2 - r) \times r, m/p = 3, \sigma^2 = 0$.

(SVP) [7], normalized iterative hard thresholding [8], and Riemannian gradient descent (RGrad) [21]. We compare these algorithms under the same settings for 100 times, and the final results are averaged over all the comparisons. We plot the per iteration normalized mean square error (NMSE) in Fig. 4. From Fig. 4, we see that TARM converges much faster than NIHT and RGrad for both Gaussian ROIL operators and partial orthogonal ROIL operators.

4) *Empirical phase transition:* The phase transition curve characterized the tradeoff between measurement rate δ and the largest rank r that an algorithm succeeds in the recovery of \mathbf{X}^* . We consider an algorithm to be successful in recovering the low-rank matrix \mathbf{X}^* when the following conditions are satisfied: 1) the normalized mean square error $\frac{\|\mathbf{X}^{(t)} - \mathbf{X}^*\|_F^2}{\|\mathbf{X}^*\|_F^2} \leq 10^{-6}$; 2) the iteration time $t < 1000$. The dimension of the manifold of $n_1 \times n_2$ matrices of rank r is $r(n_1 + n_2 - r)$ [23]. Thus, for any algorithm, the minimal number of measurements for successful recovery is $r(n_1 + n_2 - r)$, i.e., $m \geq r(n_1 + n_2 - r)$. Then, an upper bound for successful recovery is $r \leq \frac{n_1 + n_2 - \sqrt{(n_1 + n_2)^2 - 4m}}{2}$. In Fig. 5, we plot the phase transition curves of the algorithms mentioned before. From Fig. 5, we see that the phase transition curve of TARM is the closest to the upper bound and considerably higher than the curves of NIHT and RGrad.

IV. MATRIX COMPLETION

In this section, we consider TARM for the matrix completion problem, where the linear operator \mathcal{A} is a selector which selects a subset of the elements of the low-rank matrix \mathbf{X}^* . With such a choice of \mathcal{A} , the two assumptions in Section III for low-rank matrix recovery do not hold any more; see, e.g., Fig. 6. Thus, μ_t given in (13) and α_t in (15) cannot be used

iteration t	1	2	3	4	5	6	7	8
$\frac{n}{m} = 2.5$	2.4960	2.4988	2.4944	2.4948	2.4938	2.4950	2.4976	2.4968
$\frac{n}{m} = 3.3333$	3.3283	3.3273	3.3259	3.3268	3.3295	3.3267	3.3299	3.3269
$\frac{n}{m} = 5$	4.9994	4.9998	5.0034	4.9995	5.0005	5.0058	5.0078	5.0011

TABLE I. μ_t calculated by (10a) for the 1st to 8th iterations of one random realization of the algorithm with a partial orthogonal ROIL operator. $n_1 = n_2 = 1000$, $r = 30$, $\sigma = 10^{-5}$.

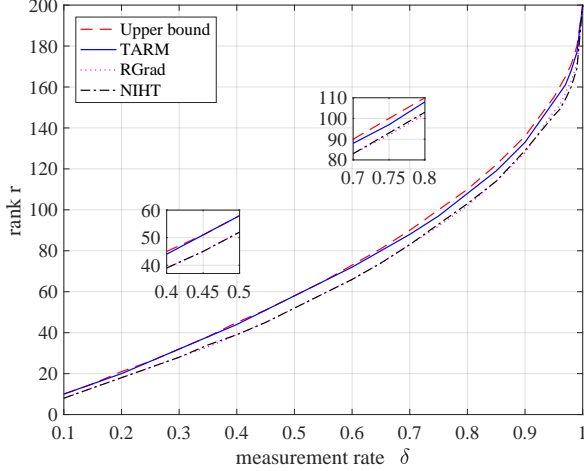


Fig. 5. The phase transition curves of various low-rank matrix recovery algorithms with a partial orthogonal ROIL operator. $n_1 = n_2 = 200$, $\sigma^2 = 0$. The region below each phase transition curve corresponds to the situation that the corresponding algorithm successfully recovers \mathbf{X}^* .

for matrix completion. We next discuss how to design μ_t and α_t for matrix completion.

A. Determining μ_t

The TARM algorithm is similar to SVP and NIHT as aforementioned. These three algorithms are all SVD based and a gradient descent step is involved at each iteration. The choice of descent step size μ_t is of key importance. In [8], [21], μ_t are chosen adaptively based on the idea of the steepest descent. Due to the similarity between TARM and NIHT, we follow the methods in [8], [21] and choose μ_t as

$$\mu_t = \frac{\|\mathcal{P}_S^{(t)}(\mathcal{A}^T(\mathbf{y} - \mathcal{A}(\mathbf{X}^{(t)})))\|_F^2}{\|\mathcal{A}(\mathcal{P}_S^{(t)}(\mathcal{A}^T(\mathbf{y} - \mathcal{A}(\mathbf{X}^{(t)}))))\|_2^2} \quad (27)$$

where $\mathcal{P}_S^{(t)} : \mathbb{R}^{n_1 \times n_2} \rightarrow \mathcal{S}$ denotes a projection operator with \mathcal{S} being a predetermined subspace of $\mathbb{R}^{n_1 \times n_2}$. The subspace \mathcal{S} can be chosen as the left singular vector space of $\mathbf{X}^{(t)}$, the right singular vector space of $\mathbf{X}^{(t)}$, or the tangent space of $\mathcal{C}(\mathbf{X}) = \frac{1}{2}\|\mathbf{y} - \mathcal{A}(\mathbf{X})\|_F^2$ at $\mathbf{X} = \mathbf{X}^{(t)}$. Let the SVD of $\mathbf{X}^{(t)}$ be $\mathbf{X}^{(t)} = \mathbf{U}^{(t)}\mathbf{\Sigma}^{(t)}(\mathbf{V}^{(t)})^T$. Then, the corresponding three projection operators are given respectively by

$$\mathcal{P}_{S_1}^{(t)}(\mathbf{X}) = \mathbf{U}^{(t)}(\mathbf{U}^{(t)})^T \mathbf{X} \quad (28a)$$

$$\mathcal{P}_{S_2}^{(t)}(\mathbf{X}) = \mathbf{X}\mathbf{V}^{(t)}(\mathbf{V}^{(t)})^T \quad (28b)$$

$$\mathcal{P}_{S_3}^{(t)}(\mathbf{X}) = \mathbf{U}^{(t)}(\mathbf{U}^{(t)})^T \mathbf{X} + \mathbf{X}\mathbf{V}^{(t)}(\mathbf{V}^{(t)})^T - \mathbf{U}^{(t)}(\mathbf{U}^{(t)})^T \mathbf{X}\mathbf{V}^{(t)}(\mathbf{V}^{(t)})^T. \quad (28c)$$

By combining (28) with (27), we obtain three different choices of μ_t . Later, we present numerical results to compare the impact of different choices of μ_t on the performance of TARM.

B. Determining α_t and c_t

The linear combination parameters α_t and c_t in TARM is difficult to evaluate since Assumptions 1 and 2 do not hold for TARM in the matrix completion problem. Recall that c_t is determined by α_t through (10c). So, we only need to determine α_t . In the following, we propose three different approaches to evaluate α_t .

The first approach is to choose α_t as in (15):

$$\alpha_t = \frac{\text{div}(\mathcal{D}(\mathbf{R}^{(t)}))}{n}. \quad (29)$$

We use the Monte Carlo method to compute the divergence. Specifically, the divergence of $\mathcal{D}(\mathbf{R}^{(t)})$ can be estimated by [22]

$$\text{div}(\mathcal{D}(\mathbf{R}^{(t)})) = \mathbb{E}_N \left[\left\langle \frac{\mathcal{D}(\mathbf{R}^{(t)} + \epsilon \mathbf{N}) - \mathcal{D}(\mathbf{R}^{(t)})}{\epsilon}, \mathbf{N} \right\rangle \right] \quad (30)$$

where $\mathbf{N} \in \mathbb{R}^{n_1 \times n_2}$ is a random Gaussian matrix with zero mean and unit variance entries, and ϵ is a small real number. The expectation in (30) can be approximated by sample mean. When the size of $\mathbf{R}^{(t)}$ is large, one sample is good enough for approximation.

We now describe the second approach. Recall that we choose c_t according to (10c) to satisfy Condition 2: $\langle \mathbf{R}^{(t)} - \mathbf{X}^*, \mathbf{X}^{(t)} - \mathbf{X}^* \rangle = 0$. Since \mathbf{X}^* is unknown, finding α_t to satisfy Condition 2 is difficult. Instead, we try to find α_t that minimizes the transformed correlation of the two estimation errors:

$$\left| \langle \mathcal{A}(\mathbf{R}^{(t)} - \mathbf{X}^*), \mathcal{A}(\mathbf{X}^{(t)} - \mathbf{X}^*) \rangle \right| \quad (31a)$$

$$= \left| \langle \mathcal{A}(\mathbf{R}^{(t)}) - \mathbf{y}, \mathcal{A}(\mathbf{X}^{(t)}) - \mathbf{y} \rangle \right| \quad (31b)$$

$$= \left| \langle \mathcal{A}(c_t(\mathbf{Z}^{(t)} - \alpha_t \mathbf{R}^{(t)})) - \mathbf{y}, \mathcal{A}(\mathbf{R}^{(t)}) - \mathbf{y} \rangle \right| \quad (31c)$$

$$= \left| \left\langle \frac{\langle \mathbf{Z}^{(t)} - \alpha_t \mathbf{R}^{(t)}, \mathbf{R}^{(t)} \rangle}{\|\mathbf{Z}^{(t)} - \alpha_t \mathbf{R}^{(t)}\|_F^2} \mathcal{A}(\mathbf{Z}^{(t)} - \alpha_t \mathbf{R}^{(t)}) - \mathbf{y}, \mathcal{A}(\mathbf{R}^{(t)}) - \mathbf{y} \right\rangle \right|. \quad (31d)$$

The minimization of (31d) over α_t can be done by an exhaustive search over a small neighbourhood of zero.

The third approach is to set α_t as the asymptotic limit given in (19a). We next provide numerical simulations to show the impact of the above three different choices of α_t on the performance of TARM.

C. Numerical Results

We compare the TARM algorithms with different choices of μ_t and α_t . We also compare TARM with the existing matrix completion algorithms, including SVP [7], NIHT [8], and RGrad [21]. The matrix form $\mathbf{A} \in \mathbb{R}^{m \times n}$ of the matrix completion operator \mathcal{A} is chosen as a random selection matrix (with randomly selected rows from a permutation matrix). The low-rank matrix $\mathbf{X}^* \in \mathbb{R}^{n_1 \times n_2}$ is generated by the multiplication of two random Gaussian matrices of size $n_1 \times r$ and $r \times n_2$.

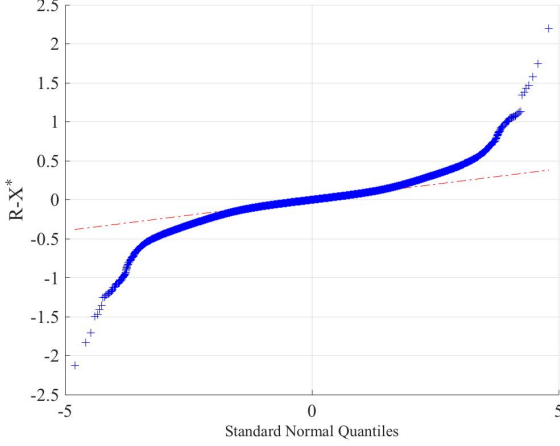


Fig. 6. The QQplots of the output error of Module A in the 5th iteration of TARM for matrix completion. Simulation settings: $n_1 = 800, n_2 = 800, r = 50, \frac{m}{n_1 n_2} = 0.3, \sigma^2 = 0$.

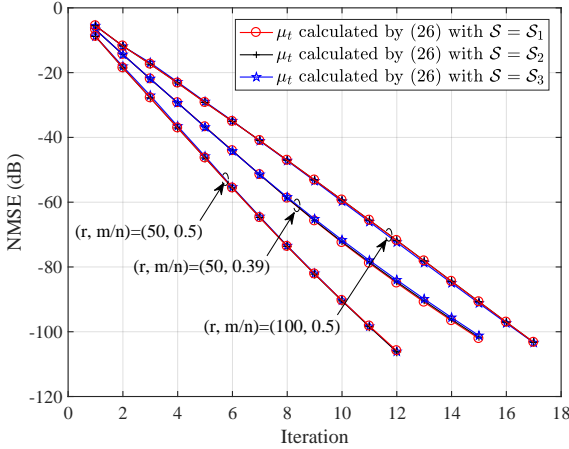


Fig. 7. Comparison of the TARM algorithms for matrix completion with different choices of μ_t . $n_1 = n_2 = 1000, \sigma^2 = 0$.

1) *Non-Gaussianity of the output error of Module A:* In Fig. 6, we plot the QQplot of the input estimation errors of Module A of TARM for matrix completion. The QQplot shows that the distribution of the estimation errors of Module A is non-Gaussian. Thus, Assumption 2 does not hold for matrix completion.

2) *Comparisons of different choices of μ_t :* We compare the TARM algorithms with μ_t in (27) and the subspace \mathcal{S} given

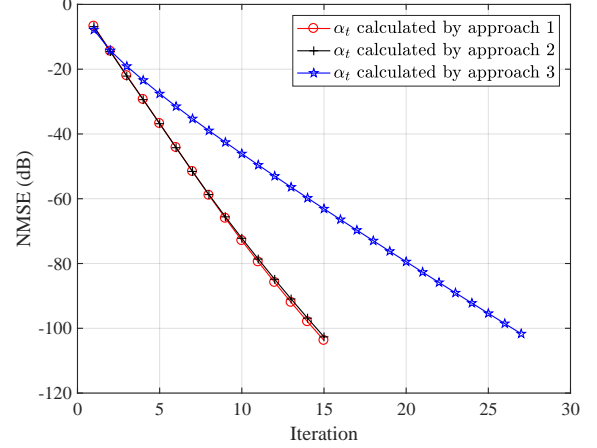


Fig. 8. Comparison of the TARM algorithms for matrix completion with different choices of α_t . $n_1 = n_2 = 1000, r = 50, \frac{m}{n_1 n_2} = 0.39, \sigma^2 = 0$.

by (28), as shown in Fig. 7. We see that the performance of TARM is not sensitive to the three choices of \mathcal{S} in (28). In the following, we always choose μ_t with \mathcal{S} given by (28a).

3) *Comparisons of different choices of α_t :* We compare the TARM algorithms with α_t given by the three different approaches in Subsection B. As shown in Fig. 8, the first approach has the best performance among the three; the second approach performance close to the first one; the third approach performs considerably worse than the first two. Note that the second approach involves exhaustive search over α_t , which is computationally involving. Thus, we henceforth choose α_t based on the first approach.

4) *Performance comparisons:* We compare TARM with the state-of-the-art algorithms for matrix completion. All the algorithms are run under the same settings for 100 random realizations. The numerical results are shown in Fig. 9. We see that TARM converges much faster than all the other algorithms.

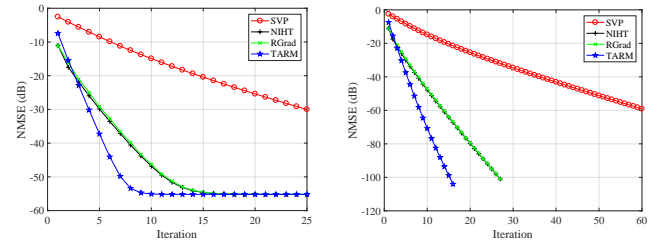


Fig. 9. Comparison of algorithms for matrix completion. Left: $n_1 = n_2 = 1000, r = 50, m/n = 0.39, \sigma^2 = 10^{-5}$. Right: $n_1 = n_2 = 1000, r = 50, m/n = 0.39, \sigma^2 = 0$.

5) *Empirical phase transition:* Similar to the case of low-rank matrix recovery. We consider an algorithm to be successful in recovering the low-rank matrix \mathbf{X}^* when the following conditions are satisfied: 1) the normalized mean square error $\frac{\|\mathbf{X}^{(t)} - \mathbf{X}^*\|_F^2}{\|\mathbf{X}^*\|_F^2} \leq 10^{-6}$; 2) the iteration time $t < 1000$. In Fig. 5, we plot the phase transition curves of the algorithms mentioned before. From Fig. 10, we see that the phase transition

of TARM is the closest to the upper bound and considerably higher than the curves of NIHT and RGrad.

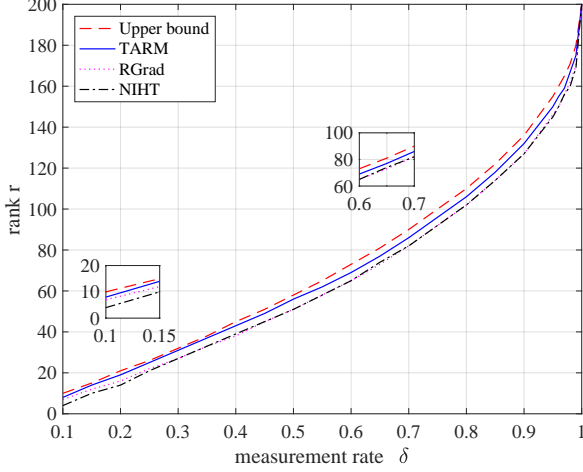


Fig. 10. The phase transition curves of various matrix completion algorithms. $n_1 = n_2 = 200, \sigma^2 = 0$. For each algorithm, the region below the phase transition curve corresponds to the successful recovery of \mathbf{X}^* .

V. CONCLUSIONS

In this paper, we proposed a low-complexity iterative algorithm termed TARM for solving the stable ARM problem. The proposed algorithm can be applied to both low-rank matrix recovery and matrix completion. For low-rank matrix recovery, the performance of TARM can be accurately characterized by the state evolution technique when ROIL operators are involved. For matrix completion, we showed that, although state evolution is not accurate, the parameters of TARM can be carefully tuned to achieve good performance. Numerical results demonstrate that TARM has competitive performance compared to other existing algorithms for both low-rank matrix recovery and matrix completion.

APPENDIX A PROOF OF LEMMA 1

We first determine μ_t . We have

$$\begin{aligned} & \langle \mathbf{R}^{(t)} - \mathbf{X}^*, \mathbf{X}^{(t-1)} - \mathbf{X}^* \rangle \\ &= \langle \mathbf{X}^{(t-1)} + \mu_t \mathcal{A}^T(\mathbf{y} - \mathcal{A}(\mathbf{X}^{(t-1)})) - \mathbf{X}^*, \mathbf{X}^{(t-1)} - \mathbf{X}^* \rangle \quad (32a) \end{aligned}$$

$$= \langle \mathbf{X}^{(t-1)} + \mu_t \mathcal{A}^T(\mathcal{A}(\mathbf{X}^*) + \mathbf{n} - \mathcal{A}(\mathbf{X}^{(t-1)})) - \mathbf{X}^*, \mathbf{X}^{(t-1)} - \mathbf{X}^* \rangle \quad (32b)$$

$$= \langle \mathbf{X}^{(t-1)} - \mathbf{X}^*, \mathbf{X}^{(t-1)} - \mathbf{X}^* \rangle - \mu_t \langle \mathcal{A}^T(\mathcal{A}(\mathbf{X}^{(t-1)} - \mathbf{X}^*)), \mathbf{X}^{(t-1)} - \mathbf{X}^* \rangle \quad (32c)$$

$$\begin{aligned} & + \mu_t \langle \mathcal{A}^T(\mathbf{n}), \mathbf{X}^{(t-1)} - \mathbf{X}^* \rangle \\ &= \langle \mathbf{X}^{(t-1)} - \mathbf{X}^*, \mathbf{X}^{(t-1)} - \mathbf{X}^* \rangle - \mu_t \langle \mathcal{A}(\mathbf{X}^{(t-1)} - \mathbf{X}^*), \mathcal{A}(\mathbf{X}^{(t-1)} - \mathbf{X}^*) \rangle \quad (32d) \\ & + \mu_t \langle \mathbf{n}, \mathcal{A}(\mathbf{X}^{(t-1)} - \mathbf{X}^*) \rangle \end{aligned}$$

where step (32a) follows by substituting $\mathbf{R}^{(t)}$ in Line 3 of Algorithm 1, and step (32d) follows by noting

$$\langle \mathcal{A}(\mathbf{B}), \mathbf{c} \rangle = \langle \mathbf{B}, \mathcal{A}^T(\mathbf{c}) \rangle \quad (33)$$

for any matrix \mathbf{B} and vector \mathbf{c} of appropriate sizes. Together with Condition 1, we obtain (10a).

We next determine α_t and c_t . First note

$$\begin{aligned} \|\mathbf{X}^{(t)} - \mathbf{R}^{(t)}\|_F^2 &= \|\mathbf{X}^{(t)} - \mathbf{X}^*\|_F^2 + \|\mathbf{X}^* - \mathbf{R}^{(t)}\|_F^2 \\ &+ 2 \langle \mathbf{X}^{(t)} - \mathbf{X}^*, \mathbf{X}^* - \mathbf{R}^{(t)} \rangle \quad (34a) \end{aligned}$$

$$= \|\mathbf{X}^{(t)} - \mathbf{X}^*\|_F^2 + \|\mathbf{X}^* - \mathbf{R}^{(t)}\|_F^2 \quad (34b)$$

where (34b) is from Condition 2 in (8). Recall that in the t -th iteration $\mathbf{R}^{(t)}$ is a function of μ_t but not of α_t and c_t . Thus, minimizing $\|\mathbf{X}^{(t)} - \mathbf{X}^*\|_F^2$ over α_t and c_t is equivalent to minimizing $\|\mathbf{X}^{(t)} - \mathbf{R}^{(t)}\|_F^2$ over α_t and c_t . For any given α_t , the optimal c_t to minimize $\|\mathbf{X}^{(t)} - \mathbf{R}^{(t)}\|_F^2 = \|c_t(\mathbf{Z}^{(t)} - \alpha_t \mathbf{R}^{(t)}) - \mathbf{R}^{(t)}\|_F^2$ is given by

$$c_t = \frac{\langle \mathbf{Z}^{(t)} - \alpha_t \mathbf{R}^{(t)}, \mathbf{R}^{(t)} \rangle}{\|\mathbf{Z}^{(t)} - \alpha_t \mathbf{R}^{(t)}\|_F^2}. \quad (35)$$

Then,

$$\begin{aligned} & \langle \mathbf{X}^{(t)} - \mathbf{X}^*, \mathbf{R}^{(t)} - \mathbf{X}^* \rangle \\ &= \langle c_t(\mathbf{Z}^{(t)} - \alpha_t \mathbf{R}^{(t)}) - \mathbf{X}^*, \mathbf{R}^{(t)} - \mathbf{X}^* \rangle \quad (36a) \end{aligned}$$

$$= \left\langle \frac{\langle \mathbf{Z}^{(t)} - \alpha_t \mathbf{R}^{(t)}, \mathbf{R}^{(t)} \rangle}{\|\mathbf{Z}^{(t)} - \alpha_t \mathbf{R}^{(t)}\|_F^2} (\mathbf{Z}^{(t)} - \alpha_t \mathbf{R}^{(t)}) - \mathbf{X}^*, \mathbf{R}^{(t)} - \mathbf{X}^* \right\rangle \quad (36b)$$

where (36a) follows by substituting $\mathbf{X}^{(t)}$ in Line 5 of Algorithm 1, and (36b) by substituting c_t in (35). Combining (36) and Condition 2, we see that α_t is the solution of the following quadratic equation:

$$a_t \alpha_t^2 + b_t \alpha_t + d_t = 0 \quad (37)$$

where a_t, b_t , and d_t are defined in (11). Therefore, α_t is given by (10a). With the above choice of c_t , we have

$$\begin{aligned} & \langle \mathbf{X}^{(t)} - \mathbf{R}^{(t)}, \mathbf{X}^{(t)} \rangle \\ &= \langle c_t(\mathbf{Z}^{(t)} - \alpha_t \mathbf{R}^{(t)}) - \mathbf{R}^{(t)}, c_t(\mathbf{Z}^{(t)} - \alpha_t \mathbf{R}^{(t)}) \rangle = 0. \quad (38) \end{aligned}$$

This orthogonality is useful in analyzing the performance of Module B.

APPENDIX B

CONVERGENCE ANALYSIS OF TARM BASED ON RIP

Without loss of generality, we assume $n_1 \leq n_2$ in this appendix. Following the convention in [8], we focus our discussion on the noiseless case, i.e., $\mathbf{n} = \mathbf{0}$.

Definition 2. (Restricted Isometry Property). Given a linear operator $\mathcal{A} : \mathbb{R}^{n_1 \times n_2} \rightarrow \mathbb{R}^m$, a minimum constant called the rank restricted isometry constant (RIC) $\delta_r(\mathcal{A}) \in (0, 1)$ exists such that

$$(1 - \delta_r(\mathcal{A})) \|\mathbf{X}\|_F^2 \leq \|\gamma \mathcal{A}(\mathbf{X})\|_2^2 \leq (1 + \delta_r(\mathcal{A})) \|\mathbf{X}\|_F^2 \quad (39)$$

for all $\mathbf{X} \in \mathbb{R}^{n_1 \times n_2}$ with $\text{rank}(\mathbf{X}) \leq r$, where $\gamma > 0$ is a constant scaling factor.

We now introduce two useful lemmas.

Lemma 3. Assume that α_{t+1} and c_{t+1} satisfy Condition 2 and Condition 3. Then,

$$\|\mathbf{X}^{(t)} - \mathbf{R}^{(t)}\|_F^2 = \frac{\|\mathbf{R}^{(t)} - \mathbf{Z}^{(t)}\|_F^2}{\frac{\|\mathbf{R}^{(t)} - \mathbf{Z}^{(t)}\|_F^2}{\|\mathbf{Z}^{(t)}\|_F^2} \alpha_t^2 + (1 - \alpha_t)^2}. \quad (40)$$

Lemma 4. Let $\mathbf{Z}^{(t)}$ be the best rank- r approximation of $\mathbf{R}^{(t)}$. Then,

$$\|\mathbf{R}^{(t)} - \mathbf{Z}^{(t)}\|_F^2 \leq \|\mathbf{X}^* - \mathbf{R}^{(t)}\|_F^2. \quad (41)$$

The proof of Lemma 3 is given in Appendix C. Lemma 4 is straightforward from the definition of the best rank- r approximation [13, p. 211-218].

Theorem 3. Assume that μ_t, α_t, c_t satisfy Conditions 1-3, and the linear operator \mathcal{A} satisfies the RIP with rank n_1 and RIC δ_{n_1} . Then,

$$\|\mathbf{X}^{(t)} - \mathbf{X}^*\|_F^2 \leq \left(\frac{1}{(1 - \alpha_t)^2} - 1 \right) \left(\frac{1 + \delta_{n_1}}{1 - \delta_{n_1}} - 1 \right)^2 \|\mathbf{X}^{(t-1)} - \mathbf{X}^*\|_F^2 \quad (42)$$

TARM guarantees to converge when RIC satisfies $\alpha_t \neq 1, \forall t$, and

$$\delta_{n_1} < \frac{1}{1 + 2\sqrt{\frac{1}{\xi} \left(\frac{1}{(1 - \alpha_{max})^2} - 1 \right)}} \quad (43)$$

where the constant ξ satisfies $0 < \xi < 1$, and $\alpha_{max} = \sup\{\alpha_t\}$.

Proof. Since $\mathbf{Z}^{(t)}$ is the best rank- r approximation of $\mathbf{R}^{(t)}$, we have $\|\mathbf{R}^{(t)}\|_F^2 \geq \|\mathbf{Z}^{(t)}\|_F^2$. Then, from Lemma 3, we obtain

$$\|\mathbf{X}^{(t)} - \mathbf{R}^{(t)}\|_F^2 \leq \frac{\|\mathbf{R}^{(t)} - \mathbf{Z}^{(t)}\|_F^2}{(1 - \alpha_t)^2}. \quad (44)$$

Then, we have

$$\|\mathbf{X}^{(t)} - \mathbf{R}^{(t)}\|_F^2 = \|\mathbf{X}^{(t)} - \mathbf{X}^* + \mathbf{X}^* - \mathbf{R}^{(t)}\|_F^2 \quad (45a)$$

$$= \|\mathbf{X}^{(t)} - \mathbf{X}^*\|_F^2 + \|\mathbf{X}^* - \mathbf{R}^{(t)}\|_F^2 + 2 \langle \mathbf{X}^{(t)} - \mathbf{X}^*, \mathbf{X}^* - \mathbf{R}^{(t)} \rangle \quad (45b)$$

$$= \|\mathbf{X}^{(t)} - \mathbf{X}^*\|_F^2 + \|\mathbf{X}^* - \mathbf{R}^{(t)}\|_F^2 \quad (45c)$$

where (45c) follows from $\langle \mathbf{X}^{(t)} - \mathbf{X}^*, \mathbf{X}^* - \mathbf{R}^{(t)} \rangle = 0$ in Condition 2, and (45d) follows from (44). Combining (41), (44), and (45), we obtain

$$\|\mathbf{X}^{(t)} - \mathbf{X}^*\|_F^2 \leq \left(\frac{1}{(1 - \alpha_t)^2} - 1 \right) \|\mathbf{R}^{(t)} - \mathbf{X}^*\|_F^2 \quad (46a)$$

$$= \left(\frac{1}{(1 - \alpha_t)^2} - 1 \right) \|\mathbf{X}^{(t-1)} + \mu_t \mathcal{A}^*(\mathbf{y} - \mathcal{A}(\mathbf{X}^{(t-1)})) - \mathbf{X}^*\|_F^2 \quad (46b)$$

$$= \left(\frac{1}{(1 - \alpha_t)^2} - 1 \right) \|(\mathcal{I} - \mu_t \mathcal{A}^* \mathcal{A})(\mathbf{X}^{(t-1)} - \mathbf{X}^*)\|_F^2. \quad (46c)$$

Since \mathcal{A} has RIP with rank n_1 and RIC δ_{n_1} , we obtain the following inequality from [24]:

$$\|(\mathcal{I} - \mu_t \mathcal{A}^* \mathcal{A})(\mathbf{X}^{(t-1)} - \mathbf{X}^*)\|_F^2 \leq \max((\mu_t(1 + \delta_{n_1}) - 1)^2, (\mu_t(1 - \delta_{n_1}) - 1)^2) \|\mathbf{X}^{(t-1)} - \mathbf{X}^*\|_F^2. \quad (47)$$

Recall that $\mu_t = \frac{\|\mathbf{X}^{(t-1)} - \mathbf{X}^*\|_F^2}{\|\mathcal{A}(\mathbf{X}^{(t-1)} - \mathbf{X}^*)\|_2^2}$ obtained by letting $\mathbf{n} = \mathbf{0}$ in (10a). From RIP, we have

$$\frac{1}{1 + \delta_{n_1}} \leq \mu_t = \frac{\|\mathbf{X}^{(t-1)} - \mathbf{X}^*\|_F^2}{\|\mathcal{A}(\mathbf{X}^{(t-1)} - \mathbf{X}^*)\|_2^2} \leq \frac{1}{1 - \delta_{n_1}}. \quad (48)$$

Then, combining (47) and (48), we have

$$\|(\mathcal{I} - \mu_t \mathcal{A}^* \mathcal{A})(\mathbf{X}^{(t-1)} - \mathbf{X}^*)\|_F^2 \leq \left(\frac{1 + \delta_{n_1}}{1 - \delta_{n_1}} - 1 \right)^2 \|\mathbf{X}^{(t-1)} - \mathbf{X}^*\|_F^2. \quad (49)$$

Combining (49) and (46), we arrive at (42).

When δ_{n_1} satisfies (41), we have

$$\|\mathbf{X}^{(t)} - \mathbf{X}^*\|_F^2 < \xi \|\mathbf{X}^{(t-1)} - \mathbf{X}^*\|_F^2 \quad (50)$$

at each iteration t . Then, TARM converges exponentially to \mathbf{X}^* . \square

We now compare the convergence rate of TARM with those of SVP and NIHT. Compared with [8, Equ. 2.11-2.14], (42) contains an extra term $\frac{1}{(1 - \alpha_t)^2} - 1$. From numerical experiments, α_t is usually close to zero, implying that TARM converges much faster than SVP and NIHT.

APPENDIX C PROOF OF THEOREM 1

For a partial orthogonal ROIL operator \mathcal{A} , the following properties hold:

$$\mathcal{A}(\mathcal{A}^T(\mathbf{a})) = \mathbf{a} \quad (51a)$$

$$\langle \mathcal{A}^T(\mathbf{a}), \mathcal{A}^T(\mathbf{b}) \rangle = \langle \mathbf{a}, \mathbf{b} \rangle. \quad (51b)$$

Then as $m, n \rightarrow \infty$ with $\frac{m}{n} \rightarrow \delta$, we have

$$\begin{aligned} & \|\mathbf{R}^{(t)} - \mathbf{X}^*\|_F^2 \\ &= \left\| \mathbf{X}^{(t)} - \mathbf{X}^* - \frac{1}{\delta} \mathcal{A}^T \mathcal{A}(\mathbf{X}^{(t)} - \mathbf{X}^*) + \mu_t \mathcal{A}^T(\mathbf{n}) \right\|_F^2 \end{aligned} \quad (52a)$$

$$\begin{aligned} &= \|\mathbf{X}^{(t)} - \mathbf{X}^*\|_F^2 + \frac{1}{\delta^2} \|\mathcal{A}^T \mathcal{A}(\mathbf{X}^{(t)} - \mathbf{X}^*)\|_F^2 \\ &\quad - \frac{2}{\delta} \|\mathcal{A}(\mathbf{X}^{(t)} - \mathbf{X}^*)\|_F^2 + \frac{1}{\delta^2} \|\mathbf{n}\|_2^2 \end{aligned} \quad (52b)$$

$$\begin{aligned} &= \|\mathbf{X}^{(t)} - \mathbf{X}^*\|_F^2 + \frac{1}{\delta^2} \|\mathcal{A}(\mathbf{X}^{(t)} - \mathbf{X}^*)\|_F^2 \\ &\quad - \frac{2}{\delta} \|\mathcal{A}(\mathbf{X}^{(t)} - \mathbf{X}^*)\|_F^2 + \frac{1}{\delta^2} \|\mathbf{n}\|_2^2 \end{aligned} \quad (52c)$$

$$\begin{aligned} &= \|\mathbf{X}^{(t)} - \mathbf{X}^*\|_F^2 + \frac{1}{\delta} \|\mathbf{X}^{(t)} - \mathbf{X}^*\|_F^2 \\ &\quad - 2 \|\mathbf{X}^{(t)} - \mathbf{X}^*\|_F^2 + \frac{1}{\delta^2} \|\mathbf{n}\|_2^2 \end{aligned} \quad (52d)$$

$$= \left(\frac{1}{\delta} - 1 \right) \|\mathbf{X}^{(t)} - \mathbf{X}^*\|_F^2 + n \sigma^2 \quad (52e)$$

where (52a) is obtained by substituting $\mathbf{R}^{(t)} = \mathbf{X}^{(t-1)} + \mu_t \mathcal{A}^T(\mathbf{y} - \mathcal{A}(\mathbf{X}^{(t-1)}))$ and $\mathbf{y} = \mathcal{A}(\mathbf{X}^*) + \mathbf{n}$, (52b) is obtained by noting that \mathbf{n} is independent of $\mathcal{A}(\mathbf{X}^{(t)} - \mathbf{X}^*)$ (ensured by Assumption 1), (52c) follows from (51b), and (52d) follows from $\frac{\|\mathcal{A}(\mathbf{X}^{(t)} - \mathbf{X}^*)\|_2^2}{\|\mathbf{X}^{(t)} - \mathbf{X}^*\|_F^2} \rightarrow \delta$ (see (13)). When $\frac{1}{n}\|\mathbf{X}^{(t)} - \mathbf{X}^*\|_F^2 \rightarrow \tau$, we have $\frac{1}{n}\|\mathbf{R}^{(t)} - \mathbf{X}^*\|_F^2 \rightarrow (\frac{1}{\delta} - 1)\tau + \sigma^2$.

We now consider the case of Gaussian ROIL operators. As $m, n \rightarrow \infty$ with $\frac{m}{n} \rightarrow \delta$, we have

$$\begin{aligned} & \|\mathbf{R}^{(t)} - \mathbf{X}^*\|_F^2 \\ &= \|\mathbf{X}^{(t)} - \mathbf{X}^*\|_F^2 + \frac{1}{\delta^2} \|\mathcal{A}^T \mathcal{A}(\mathbf{X}^{(t)} - \mathbf{X}^*)\|_F^2 \\ & \quad - \frac{2}{\delta} \|\mathcal{A}(\mathbf{X}^{(t)} - \mathbf{X}^*)\|_F^2 + \frac{1}{\delta^2} \|\mathbf{n}\|_2^2 \end{aligned} \quad (53a)$$

$$\begin{aligned} &= \|\mathbf{X}^{(t)} - \mathbf{X}^*\|_F^2 + \frac{1}{\delta^2} \|\mathbf{A}^T \mathbf{A} \text{vec}(\mathbf{X}^{(t)} - \mathbf{X}^*)\|_F^2 \\ & \quad - \frac{2}{\delta} \|\mathcal{A}(\mathbf{X}^{(t)} - \mathbf{X}^*)\|_F^2 + \frac{1}{\delta^2} \|\mathbf{n}\|_2^2 \end{aligned} \quad (53b)$$

$$\begin{aligned} &= \|\mathbf{X}^{(t)} - \mathbf{X}^*\|_F^2 + \frac{1}{\delta^2} \frac{\|\mathbf{A}^T \mathbf{A}\|_F^2}{mn} \|\text{vec}(\mathbf{X}^{(t)} - \mathbf{X}^*)\|_2^2 \\ & \quad - \frac{2}{\delta} \|\mathcal{A}(\mathbf{X}^{(t)} - \mathbf{X}^*)\|_F^2 + \frac{1}{\delta^2} \|\mathbf{n}\|_2^2 \end{aligned} \quad (53c)$$

$$\begin{aligned} &= \|\mathbf{X}^{(t)} - \mathbf{X}^*\|_F^2 + \frac{1}{\delta^2} \frac{\text{Tr}((\mathbf{A}^T \mathbf{A})^2)}{mn} \|\mathbf{X}^{(t)} - \mathbf{X}^*\|_F^2 \\ & \quad - \frac{2}{\delta} \|\mathcal{A}(\mathbf{X}^{(t)} - \mathbf{X}^*)\|_F^2 + \frac{1}{\delta^2} \|\mathbf{n}\|_2^2 \end{aligned} \quad (53d)$$

$$\begin{aligned} &= \|\mathbf{X}^{(t)} - \mathbf{X}^*\|_F^2 + (1 + \frac{1}{\delta}) \|\mathbf{X}^{(t)} - \mathbf{X}^*\|_F^2 \\ & \quad - \frac{2}{\delta} \|\mathcal{A}(\mathbf{X}^{(t)} - \mathbf{X}^*)\|_F^2 + \frac{1}{\delta^2} \|\mathbf{n}\|_2^2 \end{aligned} \quad (53e)$$

$$\begin{aligned} &= \|\mathbf{X}^{(t)} - \mathbf{X}^*\|_F^2 + (1 + \frac{1}{\delta}) \|\mathbf{X}^{(t)} - \mathbf{X}^*\|_F^2 \\ & \quad - 2 \|\mathbf{X}^{(t)} - \mathbf{X}^*\|_F^2 + \frac{1}{\delta^2} \|\mathbf{n}\|_2^2 \end{aligned} \quad (53f)$$

$$= \frac{1}{\delta} \|\mathbf{X}^{(t)} - \mathbf{X}^*\|_F^2 + n\sigma^2 \quad (53g)$$

where (53a) is from (52c), (53b) follows by utilizing the matrix form of \mathcal{A} , (53c) follows from the fact that \mathbf{V}_A is a Haar distributed orthogonal matrix independent of $\mathbf{X}^{(t)} - \mathbf{X}^*$, (53e) is obtained by noting that $\frac{1}{mn} \text{Tr}((\mathbf{A}^T \mathbf{A})^2) \rightarrow \delta + \delta^2$ since $\mathbf{A}^T \mathbf{A}$ is a Wishart matrix with variance $\frac{1}{n}$ [25, p.26], and (53f) follows by noting $\frac{\|\mathcal{A}(\mathbf{X}^{(t)} - \mathbf{X}^*)\|_2^2}{\|\mathbf{X}^{(t)} - \mathbf{X}^*\|_F^2} \rightarrow \delta$. When $\frac{1}{n}\|\mathbf{X}^{(t)} - \mathbf{X}^*\|_F^2 \rightarrow \tau$, we have $\frac{1}{n}\|\mathbf{R}^{(t)} - \mathbf{X}^*\|_F^2 \rightarrow \frac{1}{\delta}\tau + \sigma^2$.

APPENDIX D PROOF OF LEMMA 2

We first introduce two useful facts.

Fact 1: When $n_1, n_2 \rightarrow \infty$ with $n_1/n_2 = \rho, r/n_2 = \lambda$, and the singular value of $\frac{1}{\sqrt{n_2}} \mathbf{X}^*$ are $[\theta_1, \theta_2, \dots, \theta_r]$, the i -th singular value σ_i of the Gaussian noise corrupted matrix $\mathbf{R}^{(t)}$ is given by [26, equ. 9]

$$\sigma_i \xrightarrow{\text{a.s.}} \begin{cases} \sqrt{n_2 \frac{(v_t + \theta_i^2)(\rho v_t + \theta_i^2)}{\theta_i^2}} & \text{if } i \leq r \text{ and } \theta_i > \rho^{1/4} \\ \sqrt{n_2 v_t (1 + \sqrt{\rho})} & \text{otherwise} \end{cases} \quad (54)$$

where v_t is the variance of the Gaussian noise.

Fact 2: From [27, equ. 9], the divergence of a spectral function $h(\mathbf{R})$ is given by

$$\begin{aligned} \text{div}(h(\mathbf{R})) &= |n_1 - n_2| \sum_{i=1}^{\min(n_1, n_2)} \frac{h_i(\sigma_i)}{\sigma_i} + \sum_{i=1}^{\min(n_1, n_2)} h'_i(\sigma_i) \\ & \quad + 2 \sum_{i \neq j, i, j=1}^{\min(n_1, n_2)} \frac{\sigma_i h_i(\sigma_i)}{\sigma_i^2 - \sigma_j^2}. \end{aligned} \quad (55)$$

The best rank- r approximation denoiser $\mathcal{D}(\mathbf{R})$ is a spectral function with

$$\begin{cases} h_i(\sigma_i) = \sigma_i & i \leq r; \\ h_i(\sigma_i) = 0 & i > r. \end{cases} \quad (56)$$

Combining (55) and (56), the divergence of $\mathcal{D}(\mathbf{R}^{(t)})$ is given by

$$\text{div}(\mathcal{D}(\mathbf{R}^{(t)})) = |n_1 - n_2| r + r^2 + 2 \sum_{i=1}^r \sum_{j=r+1}^{\min(n_1, n_2)} \frac{\sigma_i^2}{\sigma_i^2 - \sigma_j^2}. \quad (57)$$

Further, we have

$$\begin{aligned} & \sum_{i=1}^r \sum_{j=r+1}^{\min(n_1, n_2)} \frac{\sigma_i^2}{\sigma_i^2 - \sigma_j^2} \\ & \xrightarrow{\text{a.s.}} (\min(n_1, n_2) - r) \sum_{i=1}^r \frac{\sigma_i^2}{\sigma_i^2 - (\sqrt{n_2} v_t (1 + \sqrt{\rho}))^2} \end{aligned} \quad (58a)$$

$$\begin{aligned} &= (\min(n_1, n_2) - r) \sum_{i=1}^r \frac{n_2 \frac{(v_t + \theta_i^2)(\rho v_t + \theta_i^2)}{\theta_i^2}}{\frac{n_2 (v_t + \theta_i^2)(\rho v_t + \theta_i^2)}{\theta_i^2} - n_2 v_t (1 + \sqrt{\rho})^2} \\ & \quad (58b) \end{aligned}$$

$$= (\min(n_1, n_2) - r) \sum_{i=1}^r \frac{(v_t + \theta_i^2)(\rho v_t + \theta_i^2)}{(\sqrt{\rho} v_t - \theta_i^2)^2} \quad (58c)$$

$$\begin{aligned} & \xrightarrow{\text{a.s.}} (\min(n_1, n_2) - r) r \int_0^\infty \frac{(v_t + \theta^2)(\rho v_t + \theta^2)}{(\sqrt{\rho} v_t - \theta^2)^2} p(\theta) d\theta \\ & \quad (58d) \end{aligned}$$

$$= (\min(n_1, n_2) - r) r \Delta_1(v_t) \quad (58e)$$

where both (58a) and (58b) are from (54), and (58e) follows by the definition of $\Delta_1(v_t)$. Combining (57) and (58), we obtain the asymptotic divergence of $\mathcal{D}(\mathbf{R})$ given by

$$\text{div}(\mathcal{D}(\mathbf{R})) \xrightarrow{\text{a.s.}} |n_1 - n_2| r + r^2 + 2(\min(n_1, n_2) - r) r \Delta_1(v_t) \quad (59a)$$

$$\begin{aligned} \text{and } \alpha_t &= \frac{1}{n} \text{div}(f(\mathbf{R}^{(t)})) \xrightarrow{\text{a.s.}} \left| 1 - \frac{1}{\rho} \right| \lambda + \frac{1}{\rho} \lambda^2 + \\ & 2 \left(\min \left(1, \frac{1}{\rho} \right) - \frac{\lambda}{\rho} \right) \lambda \Delta_1(v_t) = \alpha(v_t). \end{aligned}$$

Recall that $\mathbf{Z}^{(t)}$ is the best rank- r approximation of $\mathbf{R}^{(t)}$ satisfying

$$\|\mathbf{Z}^{(t)}\|_F^2 = \sum_{i=1}^r \sigma_i^2 \quad (60a)$$

$$\|\mathbf{R}^{(t)}\|_F^2 - \|\mathbf{Z}^{(t)}\|_F^2 = \sum_{i=r+1}^{n_1} \sigma_i^2. \quad (60b)$$

Then, when $m, n \rightarrow \infty$ with $\frac{m}{n} \rightarrow \delta$, we have

$$\|\mathbf{Z}^{(t)}\|_F^2 = \sum_{i=1}^r \sigma_i^2 \quad (61a)$$

$$\xrightarrow{\text{a.s.}} n_2 \sum_{i=1}^r \frac{(v + \theta_i^2)(\rho v + \theta_i^2)}{\theta_i^2} \quad (61b)$$

$$= n + \lambda \left(1 + \frac{1}{\rho}\right) nv + \lambda n v^2 \frac{1}{r} \sum_{i=1}^r \frac{1}{\theta_i^2} \quad (61c)$$

and

$$\begin{aligned} & \|\mathbf{R}^{(t)}\|_F^2 - \|\mathbf{Z}^{(t)}\|_F^2 \\ &= \|\mathbf{X}^*\|_F^2 + nv_t - \|\mathbf{Z}^{(t)}\|_F^2 \end{aligned} \quad (62a)$$

$$\xrightarrow{\text{a.s.}} nv_t - \lambda \left(1 + \frac{1}{\rho}\right) nv_t - \lambda n v_t^2 \frac{1}{r} \sum_{i=1}^r \frac{1}{\theta_i^2} \quad (62b)$$

where (61b) is from (54), (62a) is from Assumption 2, and (62b) is from (61). Then,

$$c_t = \frac{\langle \mathbf{Z}^{(t)} - \alpha_t \mathbf{R}^{(t)}, \mathbf{R}^{(t)} \rangle}{\|\mathbf{Z}^{(t)} - \alpha_t \mathbf{R}^{(t)}\|_F^2} \quad (63a)$$

$$= \frac{\langle \mathbf{Z}^{(t)}, \mathbf{R}^{(t)} \rangle - \alpha_t \|\mathbf{R}^{(t)}\|_F^2}{\|\mathbf{Z}^{(t)}\|_F^2 - 2\alpha_t \langle \mathbf{Z}^{(t)}, \mathbf{R}^{(t)} \rangle + \alpha_t^2 \|\mathbf{R}^{(t)}\|_F^2} \quad (63b)$$

$$\xrightarrow{\text{a.s.}} \frac{\|\mathbf{Z}^{(t)}\|_F^2 - \alpha_t(n + v_t n)}{\|\mathbf{Z}^{(t)}\|_F^2 - 2\alpha_t \|\mathbf{Z}^{(t)}\|_F^2 + \alpha_t^2(n + v_t n)} \quad (63c)$$

$$= \frac{n + \lambda \left(1 + \frac{1}{\rho}\right) nv_t + \lambda n v_t^2 \frac{1}{r} \sum_{i=1}^r \frac{1}{\theta_i^2} - \alpha_t(n + v_t n)}{(1 - 2\alpha_t)(n + \lambda \left(1 + \frac{1}{\rho}\right) nv_t + \lambda n v_t^2 \frac{1}{r} \sum_{i=1}^r \frac{1}{\theta_i^2}) + \alpha_t^2(n + v_t n)} \quad (63d)$$

$$= \frac{1 + \lambda \left(1 + \frac{1}{\rho}\right) v_t + \lambda v_t^2 \frac{1}{r} \sum_{i=1}^r \frac{1}{\theta_i^2} - \alpha_t(1 + v_t)}{(1 - 2\alpha_t)(1 + \lambda \left(1 + \frac{1}{\rho}\right) v_t + \lambda v_t^2 \frac{1}{r} \sum_{i=1}^r \frac{1}{\theta_i^2}) + \alpha_t^2(1 + v_t)} \quad (63e)$$

$$\xrightarrow{\text{a.s.}} \frac{1 + \lambda \left(1 + \frac{1}{\rho}\right) v_t + \lambda v_t^2 \Delta_2 - \alpha(v_t)(1 + v_t)}{(1 - 2\alpha(v_t))(1 + \lambda \left(1 + \frac{1}{\rho}\right) v_t + \lambda v_t^2 \Delta_2) + (\alpha(v_t))^2(1 + v_t)} \quad (63f)$$

$$= c(v_t) \quad (63g)$$

where (63a) is from (10c), (63c) follows from Assumption 2 that $\mathbf{R}^{(t)} = \mathbf{X}^* + \sqrt{v_t} \mathbf{W}$ with $\|\mathbf{X}^*\|_F^2 = n$, and the elements of \mathbf{W} independently drawn from $\mathcal{N}(0, 1)$, (63d) is from (60), and (63f) is from the definition of Δ_2 .

APPENDIX E PROOF OF LEMMA 3

Recall the following orthogonality relations:

$$\langle \mathbf{R}^{(t)} - \mathbf{Z}^{(t)}, \mathbf{Z}^{(t)} \rangle = 0 \quad (64a)$$

$$\langle \mathbf{R}^{(t)} - \mathbf{X}^{(t)}, \mathbf{X}^{(t)} \rangle = 0 \quad (64b)$$

where (64a) follows from $\mathbf{Z}^{(t)} = \mathcal{D}(\mathbf{R}^{(t)})$ and $\mathcal{D}(\cdot)$ is the best rank- r approximation denoiser, and (64b) follows from (38).

With the above properties, we have

$$\begin{aligned} & \|\mathbf{X}^{(t)} - \mathbf{R}^{(t)}\|_F^2 \\ &= \|\mathbf{R}^{(t)}\|_F^2 - \|\mathbf{X}^{(t)}\|_F^2 \end{aligned} \quad (65a)$$

$$= \|\mathbf{R}^{(t)}\|_F^2 - \left\| c_t (\mathbf{Z}^{(t)} - \alpha_t \mathbf{R}^{(t)}) \right\|_F^2 \quad (65b)$$

$$= \|\mathbf{R}^{(t)}\|_F^2 - \frac{\langle \mathbf{Z}^{(t)} - \alpha_t \mathbf{R}^{(t)}, \mathbf{R}^{(t)} \rangle^2}{\|\mathbf{Z}^{(t)} - \alpha_t \mathbf{R}^{(t)}\|_F^2} \quad (65c)$$

$$= \frac{\|\mathbf{R}^{(t)}\|_F^2 \|\mathbf{Z}^{(t)} - \alpha_t \mathbf{R}^{(t)}\|_F^2 - \langle \mathbf{Z}^{(t)} - \alpha_t \mathbf{R}^{(t)}, \mathbf{R}^{(t)} \rangle^2}{\|\mathbf{Z}^{(t)} - \alpha_t \mathbf{R}^{(t)}\|_F^2} \quad (65d)$$

$$= \frac{\|\mathbf{R}^{(t)}\|_F^2 \|\mathbf{Z}^{(t)}\|_F^2 - \langle \mathbf{Z}^{(t)}, \mathbf{R}^{(t)} \rangle^2}{\|\mathbf{Z}^{(t)} - \alpha_t \mathbf{R}^{(t)}\|_F^2} \quad (65e)$$

$$= \frac{\|\mathbf{R}^{(t)}\|_F^2 \|\mathbf{Z}^{(t)}\|_F^2 - \|\mathbf{Z}^{(t)}\|_F^4}{\|\mathbf{Z}^{(t)} - \alpha_t \mathbf{R}^{(t)}\|_F^2} \quad (65f)$$

$$= \frac{\|\mathbf{R}^{(t)}\|_F^2 - \|\mathbf{Z}^{(t)}\|_F^2}{\frac{\|\mathbf{R}^{(t)}\|_F^2 - \|\mathbf{Z}^{(t)}\|_F^2}{\|\mathbf{Z}^{(t)}\|_F^2} \alpha_t^2 + (1 - \alpha_t)^2} \quad (65g)$$

$$= \frac{\|\mathbf{R}^{(t)} - \mathbf{Z}^{(t)}\|_F^2}{\frac{\|\mathbf{R}^{(t)}\|_F^2 - \|\mathbf{Z}^{(t)}\|_F^2}{\|\mathbf{Z}^{(t)}\|_F^2} \alpha_t^2 + (1 - \alpha_t)^2} \quad (65h)$$

where (65a) follows from (64b), (65b) follows by substituting $\mathbf{X}^{(t)}$ in Line 5 of Algorithm 1, (65c) follows by substituting c_t in (10c), and (65f-65h) follow from (64a). This concludes the proof of Lemma 3.

APPENDIX F PROOF OF THEOREM 2

From Condition 2 in (8) and Assumption 2, we have¹

$$\langle \mathbf{R}^{(t)} - \mathbf{X}^*, \mathbf{X}^* \rangle = 0 \quad (66a)$$

$$\langle \mathbf{R}^{(t)} - \mathbf{X}^*, \mathbf{X}^{(t)} - \mathbf{X}^* \rangle = 0. \quad (66b)$$

Then,

$$\begin{aligned} & \|\mathbf{X}^{(t)} - \mathbf{X}^*\|_F^2 \\ &= \|\mathbf{X}^{(t)} - \mathbf{R}^{(t)}\|_F^2 - 2 \langle \mathbf{X}^{(t)} - \mathbf{R}^{(t)}, \mathbf{R}^{(t)} - \mathbf{X}^* \rangle \\ & \quad + \|\mathbf{R}^{(t)} - \mathbf{X}^*\|_F^2 \end{aligned} \quad (67a)$$

$$= \|\mathbf{R}^{(t)} - \mathbf{X}^{(t)}\|_F^2 - \|\mathbf{R}^{(t)} - \mathbf{X}^*\|_F^2 \quad (67b)$$

$$= \frac{\|\mathbf{R}^{(t)}\|_F^2 - \|\mathbf{Z}^{(t)}\|_F^2}{\frac{\|\mathbf{R}^{(t)}\|_F^2 - \|\mathbf{Z}^{(t)}\|_F^2}{\|\mathbf{Z}^{(t)}\|_F^2} \alpha_t^2 + (1 - \alpha_t)^2} - \|\mathbf{R}^{(t)} - \mathbf{X}^*\|_F^2 \quad (67c)$$

$$\xrightarrow{\text{a.s.}} \frac{nv_t - \lambda \left(1 + \frac{1}{\rho}\right) nv_t - \lambda n v_t^2 \Delta_2}{\frac{v_t - \lambda \left(1 + \frac{1}{\rho}\right) v_t - \lambda v_t^2 \Delta_2}{1 + \lambda \left(1 + \frac{1}{\rho}\right) v_t + \lambda v_t^2 \Delta_2} (\alpha(v_t))^2 + (1 - \alpha(v_t))^2} - nv_t \quad (67d)$$

where (67b) is from (66b), (67c) follows from (65), and (67d) follows from (61) and (62) and Assumption 2. Therefore, (23) holds, which concludes the proof of Theorem 2.

¹In fact, as $n_1, n_2, r \rightarrow \infty$ with $\frac{n_1}{n_2} \rightarrow \rho$ and $\frac{r}{n_2} \rightarrow \lambda$, the approximation in (14) become accurate, i.e. $\alpha_t = \frac{n_2}{n} \text{div}(\mathcal{D}(\mathbf{R}^{(t)}))$ asymptotically satisfies Condition 2. Thus, (66b) asymptotically holds.

REFERENCES

- [1] E. J. Candes and Y. Plan, "Matrix completion with noise," *Proc. IEEE*, vol. 98, no. 6, pp. 925–936, June 2010.
- [2] M. A. Davenport and J. Romberg, "An overview of low-rank matrix recovery from incomplete observations," *IEEE J. Sel. Topics Signal Process.*, vol. 10, no. 4, pp. 608–622, Mar. 2016.
- [3] B. Recht, M. Fazel, and P. A. Parrilo, "Guaranteed minimum-rank solutions of linear matrix equations via nuclear norm minimization," *SIAM Rev.*, vol. 52, no. 3, pp. 471–501, Aug. 2010.
- [4] Z. Liu and L. Vandenberghe, "Interior-point method for nuclear norm approximation with application to system identification," *SIAM J. Matrix Anal. Appl.*, vol. 31, no. 3, pp. 1235–1256, Nov. 2009.
- [5] J.-F. Cai, E. J. Candès, and Z. Shen, "A singular value thresholding algorithm for matrix completion," *SIAM J. Optim.*, vol. 20, no. 4, pp. 1956–1982, Mar. 2010.
- [6] K.-C. Toh and S. Yun, "An accelerated proximal gradient algorithm for nuclear norm regularized linear least squares problems," *Pacific J. Optim.*, vol. 6, no. 615–640, p. 15, Mar. 2010.
- [7] P. Jain, R. Meka, and I. S. Dhillon, "Guaranteed rank minimization via singular value projection," in *Advances in Neural Information Processing Systems Conference*, Hyatt Regency, Vancouver Canada, pp. 937–945, Dec. 2010.
- [8] J. Tanner and K. Wei, "Normalized iterative hard thresholding for matrix completion," *SIAM J. Sci. Comput.*, vol. 35, no. 5, pp. S104–S125, Oct. 2013.
- [9] T. Blumensath and M. E. Davies, "Iterative hard thresholding for compressed sensing," *Applied and computational harmonic analysis*, vol. 27, no. 3, pp. 265–274, Nov. 2009.
- [10] P. Jain, P. Netrapalli, and S. Sanghavi, "Low-rank matrix completion using alternating minimization," in *Proceedings of the Forty-fifth Annual ACM Symposium on Theory of Computing*, Palo Alto, CA, pp. 665–674, June 2013.
- [11] J. Ma, X. Yuan, and L. Ping, "Turbo compressed sensing with partial DFT sensing matrix," *IEEE Signal Process. Lett.*, vol. 22, no. 2, pp. 158–161, Feb. 2015.
- [12] Z. Xue, J. Ma, and X. Yuan, "Denoising-based turbo compressed sensing," *IEEE Access*, vol. 5, pp. 7193–7204, Apr. 2017.
- [13] C. Eckart and G. Young, "The approximation of one matrix by another of lower rank," *Psychometrika*, vol. 1, no. 3, pp. 211–218, Mar. 1936.
- [14] E. J. Candès and B. Recht, "Exact matrix completion via convex optimization," *Found. Comput. Math.*, vol. 9, no. 6, p. 717–772, Apr. 2009.
- [15] J. Ma and L. Ping, "Orthogonal AMP," *IEEE Access*, vol. 5, pp. 2020–2033, Jan. 2017.
- [16] S. Rangan, P. Schniter, and A. K. Fletcher, "Vector approximate message passing," in *Proceedings of IEEE Information International Symposium on Theory (ISIT)*, Aachen, Germany, pp. 1588–1592, Aug. 2017.
- [17] K. Takeuchi, "Rigorous dynamics of expectation-propagation-based signal recovery from unitarily invariant measurements," *arXiv preprint arXiv:1701.05284*, 2017.
- [18] M. Bayati and A. Montanari, "The dynamics of message passing on dense graphs, with applications to compressed sensing," *IEEE Trans. Info. Theory*, vol. 57, no. 2, pp. 764–785, Jan. 2011.
- [19] R. Berthier, A. Montanari, and P. M. Nguyen, "State evolution for approximate message passing with non-separable functions," *arXiv preprint arXiv:1708.03950*, 2017.
- [20] C. M. Stein, "Estimation of the mean of a multivariate normal distribution," *Ann. STAT.*, pp. 1135–1151, 1981.
- [21] K. Wei, J.-F. Cai, T. F. Chan, and S. Leung, "Guarantees of riemannian optimization for low rank matrix recovery," *SIAM J. Matrix Anal. Appl.*, vol. 37, no. 3, pp. 1198–1222, Sep. 2016.
- [22] C. Metzler, A. Maleki, and R. G. Baraniuk, "From denoising to compressed sensing," *IEEE Trans. Info. Theory*, vol. 62, no. 9, pp. 5117–5144, Apr. 2016.
- [23] B. Vandereycken, "Low-rank matrix completion by riemannian optimization," *SIAM J. Optim.*, vol. 23, no. 2, pp. 1214–1236, June 2013.
- [24] A. Kyrillidis and V. Cevher, "Matrix recipes for hard thresholding methods," *J. Math. Imag. Vision*, vol. 48, no. 2, pp. 235–265, Feb. 2014.
- [25] A. M. Tulino, S. Verdú *et al.*, "Random matrix theory and wireless communications", Now Publishers, 2004.
- [26] F. Benaych-Georges and R. R. Nadakuditi, "The singular values and vectors of low rank perturbations of large rectangular random matrices," *J. Multivariate Anal.*, vol. 111, pp. 120–135, Oct. 2012.
- [27] E. J. Candes, C. A. Sing-Long, and J. D. Trzasko, "Unbiased risk estimates for singular value thresholding and spectral estimators," *IEEE Trans. Signal Process.*, vol. 61, no. 19, pp. 4643–4657, June 2013.